Constraining anomalous Higgs boson couplings to virtual photons

Jeffrey Davis¹, Andrei V. Gritsan¹, Lucas S. Mandacarú Guerra¹, Savvas Kyriacou¹, Lucas S. Mandacarú Guerra¹, Savvas Kyriacou¹, Jeffrey Roskes, and Markus Schulze^{2,¶}

¹Department of Physics and Astronomy, Johns Hopkins University, Baltimore, Maryland 21218, USA ²Institut für Physik, Humboldt-Universität zu Berlin, D-12489 Berlin, Germany

(Received 27 September 2021; accepted 28 March 2022; published 25 May 2022)

We present a study of Higgs boson production in vector boson fusion and in association with a vector boson and its decay to two vector bosons, with a focus on the treatment of virtual loops and virtual photons. Our analysis is performed with the JHU generator framework. Comparisons are made to several other frameworks, and the results are expressed in terms of an effective field theory. New features of this study include a proposal on how to handle singularities involving Higgs boson decays to light fermions via photons, calculation of the partial Higgs boson width in the presence of anomalous couplings to photons, a comparison of the next-to-leading-order electroweak corrections to effects from effective couplings, and phenomenological observations regarding the special role of intermediate photons in analysis of LHC data in the effective field theory framework. Some of these features are illustrated with projections for experimental measurements with the full LHC and HL-LHC datasets.

DOI: 10.1103/PhysRevD.105.096027

I. INTRODUCTION

The large amount of data analyzed by the ATLAS and CMS experiments on the Large Hadron Collider (LHC) is consistent with the predictions of the standard model (SM) of particle physics. Among the measurements performed, the discovery and characterization of the Higgs (H) boson have been crucial in completing the SM [1-3]. Yet, open questions remain, such as the low value of the H boson's mass, its Yukawa coupling hierarchy, the source of CP violation required for matter abundance, and the connection of the SM to other cosmological observations.

Studies of electroweak production (VBF and VH) and decay $(H \rightarrow VV)$ of the H boson probe HVV interactions over a large range of momentum transfer, which can expose possible new particles that couple through loops. Such electroweak processes lead to rich information in kinematic distributions of the H boson decay products and associated particles. Analysis of such distributions can shed light on the nature of the HVV interactions and has been discussed

Published by the American Physical Society under the terms of the Creative Commons Attribution 4.0 International license. Further distribution of this work must maintain attribution to the author(s) and the published article's title, journal citation, and DOI. Funded by SCOAP³.

extensively [4–45]. Such studies can be naturally performed within the effective field theory (EFT) framework, with examples of application to LHC data documented in Refs. [3,46–60].

In our earlier studies using the JHU generator framework [19,23,28,38,45,61], we relied on dedicated Monte Carlo simulation, and demonstrated optimal discrimination, reweighting techniques, and analysis of a bosonic resonance with the most general anomalous couplings. We build upon this framework of the JHU generator and MELA analysis package with the goal of demonstrating its application to the H boson's interactions in electroweak processes with massless vector bosons, such as in $HZ\gamma$, $H\gamma\gamma$, and Hgg vertices. Such couplings are generated in the SM through loops of SM particles. They also lead to divergence of fixed-order calculations for virtual γ^* states when the four-momentum squared $q_{\gamma^*}^2$ approaches zero. In the perturbative expansion, such terms are poorly defined at low values of q^2 . Some prior discussion of this effect can be found in Refs. [40-44,62].

We review the parametrization of anomalous H boson couplings in Sec. II and discuss applications of the JHU generator framework to EFT studies in Sec. III. In Sec. IV, the partial H boson width and production cross sections are calculated in the presence of anomalous couplings to massless vector bosons. In Sec. V, the treatment of the nextto-leading-order (NLO) electroweak (EW) effects is discussed. In Sec. VI, we make a proposal on how to handle singularities involving intermediate photons in the H boson decays. In Sec. VII, several phenomenological observations are made in application to LHC data.

jdavi231@jhu.edu gritsan@jhu.edu

lmandac1@jhu.edu

skyriac2@jhu.edu

hroskes@jhu.edu

markus.schulze@physik.hu-berlin.de

II. PARAMETRIZATION OF ANOMALOUS INTERACTIONS

We start with the HVV scattering amplitude of a spinzero boson H and two vector bosons VV with polarization vectors and momenta ε_1^{μ} , q_1^{μ} , and ε_2^{μ} , q_2^{μ} . The amplitude is parametrized by

$$\begin{split} A(HV_1V_2) = & \frac{1}{v} \left\{ M_{V_1}^2 \left(g_1^{VV} + \frac{\kappa_1^{VV} q_1^2 + \kappa_2^{VV} q_2^2}{(\Lambda_1^{VV})^2} \right. \right. \\ & \left. + \frac{\kappa_3^{VV} (q_1 + q_2)^2}{(\Lambda_Q^{VV})^2} + \frac{2q_1 \cdot q_2}{M_{V_1}^2} g_2^{VV} \right) (\varepsilon_1 \cdot \varepsilon_2) \right. \\ & \left. - 2g_2^{VV} (\varepsilon_1 \cdot q_2) (\varepsilon_2 \cdot q_1) - 2g_4^{VV} \varepsilon_{\varepsilon_1 \varepsilon_2 q_1 q_2} \right\}, \quad (1) \end{split}$$

where v is the vacuum expectation value, under the conventions $\varepsilon_{0123}=+1$ and $(q^{\mu})=(E,\vec{q})$. This amplitude represents the three possible tensor structures of the H

boson's interaction with two vector bosons, with expansion of the terms up to q_i^2 . By symmetry we have $\kappa_1^{ZZ} = \kappa_2^{ZZ}$, but we do not enforce $\kappa_1^{WW} = \kappa_2^{WW}$ for W^\pm bosons. Note that $\kappa_1^{\gamma\gamma} = \kappa_2^{\gamma\gamma} = \kappa_1^{\rm gg} = \kappa_2^{\rm gg} = \kappa_1^{Z\gamma} = 0$, while $\kappa_2^{Z\gamma}/(\Lambda_1^{Z\gamma})^2$ may contribute. The coupling $\kappa_3^{VV}/(\Lambda_Q^{VV})^2$ allows for scenarios which violate the gauge symmetries of the SM.

An effective HVV interaction may be generated by loops of fermions, in which case the couplings κ_f and $\tilde{\kappa}_f$ describe the H boson interactions as

$$A(Hf\bar{f}) = -\frac{m_f}{v}\bar{\psi}_f(\kappa_f + i\tilde{\kappa}_f\gamma_5)\psi_f, \qquad (2)$$

where $\bar{\psi}_f$ and ψ_f are the Dirac spinors and m_f is the fermion mass. For the SM fermions, $(\kappa_f, \tilde{\kappa}_f) = (1, 0)$.

The equivalent Lagrangian for *H* boson interactions with gauge bosons (in the mass eigenstate parametrization) reads

$$\begin{split} \mathcal{L}_{\text{hvv}} &= \frac{h}{v} \left[M_Z^2 (1 + \delta c_z) Z_\mu Z^\mu + \frac{M_Z^2}{v^2} c_{zz} Z_{\mu\nu} Z^{\mu\nu} + \frac{e^2}{s_w^2} c_{z\square} Z_\mu \partial_\nu Z^{\mu\nu} + \frac{M_Z^2}{v^2} \tilde{c}_{zz} Z^{\mu\nu} \tilde{Z}_{\mu\nu} + 2 M_W^2 (1 + \delta c_w) W_\mu^+ W^{-\mu} \right. \\ &\quad + 2 \frac{M_W^2}{v^2} c_{ww} W_{\mu\nu}^+ W^{-\mu\nu} + \frac{e^2}{s_w^2} c_{w\square} (W_\mu^- \partial_\nu W^{+\mu\nu} + \text{H.c.}) + \frac{e^2}{2s_w^2} \tilde{c}_{ww} W^{+\mu\nu} \tilde{W}_{\mu\nu}^- + \frac{e^2}{2s_w c_w} c_{z\gamma} Z_{\mu\nu} A^{\mu\nu} + \frac{e^2}{2s_w c_w} \tilde{c}_{z\gamma} Z_{\mu\nu} \tilde{A}^{\mu\nu} \right. \\ &\quad + \frac{e^2}{s_w c_w} c_{\gamma\square} Z_\mu \partial_\nu A^{\mu\nu} + c_{\gamma\gamma} \frac{e^2}{4} A_{\mu\nu} A^{\mu\nu} + \tilde{c}_{\gamma\gamma} \frac{e^2}{4} A^{\mu\nu} \tilde{A}_{\mu\nu} + c_{gg} \frac{g_s^2}{4} G_{\mu\nu}^a G^{a\mu\nu} + \tilde{c}_{gg} \frac{g_s^2}{4} G^{a\mu\nu} \tilde{G}_{\mu\nu}^a \right], \end{split} \tag{3}$$

in accordance with Eq. (II.2.20) in Ref. [39], where $e^2 = 4\pi\alpha$ and $g_s^2 = 4\pi\alpha_s$ are the squared electromagnetic and strong coupling constants, respectively, and $s_w = \sqrt{1-c_w^2}$ is the sine of the weak mixing angle. The covariant derivative used to derive this expression is $D_\mu = \partial_\mu - i\frac{e}{2s_w}\sigma^i W_\mu^i - i\frac{e}{2c_w}B_\mu$ [39,63]. We note that the convention $\varepsilon_{0123} = +1$ defines the relative sign of the CP-odd \tilde{c}_i and CP-even c_i couplings [45], while the relative sign in front

of the W^i_{μ} and B_{μ} terms in the covariant derivative defines the sign of the $Z\gamma$ couplings relative to the ZZ and $\gamma\gamma$. The latter could be viewed as the sign of s_w , if a different convention is adopted.

The generality of our amplitude parametrization allows us to uniquely represent each EFT coefficient in Eq. (3) by an anomalous coupling in Eq. (1).

$$\begin{split} \delta c_z &= \frac{1}{2} g_1^{ZZ} - 1, \qquad c_{zz} = -\frac{2 s_w^2 c_w^2}{e^2} g_2^{ZZ}, \qquad c_{z\square} = \frac{M_Z^2 s_w^2}{e^2} \frac{\kappa_1^{ZZ}}{(\Lambda_1^{ZZ})^2}, \qquad \tilde{c}_{zz} = -\frac{2 s_w^2 c_w^2}{e^2} g_4^{ZZ}, \\ \delta c_w &= \frac{1}{2} g_1^{WW} - 1, \qquad c_{ww} = -\frac{2 s_w^2}{e^2} g_2^{WW}, \qquad c_{w\square} = \frac{M_W^2 s_w^2}{e^2} \frac{\kappa_1^{WW}}{(\Lambda_1^{WW})^2}, \qquad \tilde{c}_{ww} = -\frac{2 s_w^2}{e^2} g_4^{WW}, \\ c_{z\gamma} &= -\frac{2 s_w c_w}{e^2} g_2^{Z\gamma}, \qquad \tilde{c}_{z\gamma} = -\frac{2 s_w c_w}{e^2} g_4^{Z\gamma}, \qquad c_{\gamma\square} = \frac{s_w c_w}{e^2} \frac{M_Z^2}{(\Lambda_1^{Z\gamma})^2} \kappa_2^{Z\gamma}, \\ c_{\gamma\gamma} &= -\frac{2}{e^2} g_2^{\gamma\gamma}, \qquad \tilde{c}_{\gamma\gamma} = -\frac{2}{e^2} g_4^{\gamma\gamma}, \qquad c_{gg} = -\frac{2}{g_s^2} g_2^{gg}, \qquad \tilde{c}_{gg} = -\frac{2}{g_s^2} g_4^{gg}. \end{split}$$

¹In the actual parametrization of the JHUGen framework discussed in Sec. III and Refs. [19,23,28,38,45,61], the $D_{\mu}=\partial_{\mu}-i\frac{e}{2s_{w}}\sigma^{i}W_{\mu}^{i}+i\frac{e}{2c_{w}}B_{\mu}$ convention was adopted for historical reasons. A transformation $g_{i}^{Z\gamma}\to-g_{i}^{Z\gamma}$ or $\kappa_{i}^{Z\gamma}\to-\kappa_{i}^{Z\gamma}$ of the input parameters in this framework would lead to the convention $D_{\mu}=\partial_{\mu}-i\frac{e}{2s_{w}}\sigma^{i}W_{\mu}^{i}-i\frac{e}{2c_{w}}B_{\mu}$, which is needed for consistent application of the formalism discussed in this paper.

Note that not every anomalous coupling in Eq. (1) has a corresponding term in the EFT Lagrangian of Eq. (3). For example, the term $\kappa_3^{VV}/(\Lambda_Q^{VV})^2$ is not gauge invariant and is not present in Eq. (3). Similarly, $\kappa_1^{WW}=\kappa_2^{WW}$ due to charge symmetry.

So far we have discussed the H boson interactions without considering additional symmetries. The $SU(3) \times SU(2) \times U(1)$ symmetry of the standard model effective field theory (SMEFT) [64–67] is a motivated framework which allows relating EFT operators. Not all of the EFT coefficients are independent when limiting the discussion to dimension-six interactions with this symmetry. The linear relations for the dependent coefficients can be found in Ref. [39] and they translate into relations amongst our anomalous couplings as follows:

$$g_1^{WW} = g_1^{ZZ} + \frac{\Delta M_W}{M_W},\tag{5}$$

$$g_2^{WW} = c_w^2 g_2^{ZZ} + s_w^2 g_2^{\gamma\gamma} + 2s_w c_w g_2^{Z\gamma}, \tag{6}$$

$$g_4^{WW} = c_w^2 g_4^{ZZ} + s_w^2 g_4^{\gamma \gamma} + 2s_w c_w g_4^{Z\gamma}, \tag{7}$$

$$\begin{split} \frac{\kappa_1^{WW}}{(\Lambda_1^{WW})^2} (c_w^2 - s_w^2) &= \frac{\kappa_1^{ZZ}}{(\Lambda_1^{ZZ})^2} + 2s_w^2 \frac{g_2^{\gamma\gamma} - g_2^{ZZ}}{M_Z^2} \\ &+ 2\frac{s_w}{c_w} (c_w^2 - s_w^2) \frac{g_2^{Z\gamma}}{M_Z^2}, \end{split} \tag{8}$$

$$\begin{split} \frac{\kappa_{2}^{Z\gamma}}{(\Lambda_{1}^{Z\gamma})^{2}}(c_{w}^{2}-s_{w}^{2}) &= 2s_{w}c_{w}\bigg(\frac{\kappa_{1}^{ZZ}}{(\Lambda_{1}^{ZZ})^{2}} + \frac{g_{2}^{\gamma\gamma}-g_{2}^{ZZ}}{M_{Z}^{2}}\bigg) \\ &+ 2(c_{w}^{2}-s_{w}^{2})\frac{g_{2}^{Z\gamma}}{M_{Z}^{2}}. \end{split} \tag{9}$$

The Lagrangian for H boson interactions with gauge bosons can be written in the Warsaw basis [68] which preserves the $SU(3) \times SU(2) \times U(1)$ symmetry of SMEFT. The relationship between operators in the Warsaw basis and the mass-eigenstate basis is discussed in Sec. III.

III. THE JHU GENERATOR FRAMEWORK AND THE EFT BASES

The JHU generator framework (JHUGen) includes a Monte Carlo generator and matrix element techniques for optimal analysis of the data. It is built upon the earlier developed framework of the JHU generator and MELA analysis package [19,23,28,38,45,61] and extensively uses matrix elements provided by MCFM [69–73]. The SM processes in MCFM are extended to add the most general scalar and gauge couplings and possible additional states. This framework includes many options for production and decay of the *H* boson, which include the gluon fusion, vector boson fusion, and associated production with a

vector boson (VH) in both on-shell H and off-shell H^* production [45]. In the off-shell case, interference with background processes or a second resonance is included. The processes with direct sensitivity to fermion $Hf\bar{f}$ couplings, such as $t\bar{t}H$, $b\bar{b}H$, tqH, tWH, or $H \to \tau^+\tau^-$, are discussed in Refs. [38,61].

The JHUGen framework was adopted in Run-I analyses using LHC data [2,3,46-50,52,74-77] and employed in recent Run-II measurements of the HVV anomalous couplings from the first joint analysis of on-shell production and decay [53,58], from the first joint analysis of on-shell and off-shell H boson production [57], for the first measurement of the CP structure of the Yukawa interaction between the H boson and the top quark [78], in the search for a second resonance in interference with the continuum background [79,80], and in EFT approach to the HVV, Hgg, and $Hf\bar{f}$ interactions [60].

A. EFT basis considerations

The framework is based on the amplitude parametrization in Eqs. (1) and (2). In order to simplify translation between different coupling conventions and operator bases, including the Higgs and Warsaw bases, within the JHU generator framework, we provide the JHUGenLexicon program, which includes an interface to the generator and matrix element library and can also be used for standalone or other applications [45]. The relationship of the amplitude parametrization to the mass eigenstate basis of the EFT formulations in Eq. (3) is performed through the simple linear relationship in Eq. (4). The functionality of this program is similar to ROSETTA [81], but it is limited in scope to application to the *H* boson interactions and provides additional options to introduce certain symmetries or constraints, as illustrated below.

We count five CP-even and three CP-odd independent electroweak HVV operators, as well as one CP-even and one CP-odd Hgg operators in the mass-eigenstate basis in Sec. II. The same number of independent H boson operators exists in the Warsaw basis. The relationship between the six CP-even operators is quoted explicitly in Eq. (14) of Ref. [81]. This relationship is direct, with the exception of the δv parameter defined in the Warsaw basis in Eq. (15) of Ref. [81]. One could remove an extra parameter from transformation with constraints from precision electroweak data. For example, we can set $\Delta M_W = 0$ in Eq. (5), because M_W is measured precisely. This allows us to express δv through the other HVV operators in the Warsaw basis. The JHUGenLexicon program provides such an option and the following studies in this paper will be presented with such a constraint.

With the above symmetries and constraints, including $\Delta M_W = 0$, the translation between the Warsaw basis and the independent amplitude coefficients is

$$\begin{split} \delta g_{1}^{ZZ} &= \frac{v^{2}}{\Lambda^{2}} \left(2C_{H\Box} + \frac{6e^{2}}{s_{w}^{2}} C_{HWB} + \left(\frac{3c_{w}^{2}}{2s_{w}^{2}} - \frac{1}{2} \right) C_{HD} \right), \\ \kappa_{1}^{ZZ} &= \frac{v^{2}}{\Lambda^{2}} \left(-\frac{2e^{2}}{s_{w}^{2}} C_{HWB} + \left(1 - \frac{1}{2s_{w}^{2}} \right) C_{HD} \right), \\ g_{2}^{ZZ} &= -2 \frac{v^{2}}{\Lambda^{2}} \left(s_{w}^{2} C_{HB} + c_{w}^{2} C_{HW} + s_{w} c_{w} C_{HWB} \right), \\ g_{2}^{Z\gamma} &= -2 \frac{v^{2}}{\Lambda^{2}} \left(s_{w} c_{w} (C_{HW} - C_{HB}) + \frac{1}{2} (s_{w}^{2} - c_{w}^{2}) C_{HWB} \right), \\ g_{2}^{\gamma\gamma} &= -2 \frac{v^{2}}{\Lambda^{2}} \left(c_{w}^{2} C_{HB} + s_{w}^{2} C_{HW} - s_{w} c_{w} C_{HWB} \right), \\ g_{2}^{gg} &= -2 \frac{v^{2}}{\Lambda^{2}} C_{HG}, \\ g_{4}^{ZZ} &= -2 \frac{v^{2}}{\Lambda^{2}} \left(s_{w}^{2} C_{H\tilde{B}} + c_{w}^{2} C_{H\tilde{W}} + s_{w} c_{w} C_{H\tilde{W}B} \right), \\ g_{4}^{\gamma\gamma} &= -2 \frac{v^{2}}{\Lambda^{2}} \left(s_{w} c_{w} (C_{H\tilde{W}} - C_{H\tilde{B}}) + \frac{1}{2} (s_{w}^{2} - c_{w}^{2}) C_{H\tilde{W}B} \right), \\ g_{4}^{\gamma\gamma} &= -2 \frac{v^{2}}{\Lambda^{2}} \left(c_{w}^{2} C_{H\tilde{B}} + s_{w}^{2} C_{H\tilde{W}} - s_{w} c_{w} C_{H\tilde{W}B} \right), \\ g_{4}^{gg} &= -2 \frac{v^{2}}{\Lambda^{2}} \left(c_{w}^{2} C_{H\tilde{B}} + s_{w}^{2} C_{H\tilde{W}} - s_{w} c_{w} C_{H\tilde{W}B} \right), \\ g_{4}^{gg} &= -2 \frac{v^{2}}{\Lambda^{2}} \left(c_{W}^{2} C_{H\tilde{B}} + s_{w}^{2} C_{H\tilde{W}} - s_{w} c_{w} C_{H\tilde{W}B} \right), \\ g_{4}^{gg} &= -2 \frac{v^{2}}{\Lambda^{2}} \left(c_{W}^{2} C_{H\tilde{B}} + s_{w}^{2} C_{H\tilde{W}} - s_{w} c_{w} C_{H\tilde{W}B} \right), \\ g_{4}^{gg} &= -2 \frac{v^{2}}{\Lambda^{2}} \left(c_{W}^{2} C_{H\tilde{B}} + s_{w}^{2} C_{H\tilde{W}} - s_{w} c_{w} C_{H\tilde{W}B} \right), \\ g_{4}^{gg} &= -2 \frac{v^{2}}{\Lambda^{2}} \left(c_{W}^{2} C_{H\tilde{B}} + s_{w}^{2} C_{H\tilde{W}} - s_{w} c_{w} C_{H\tilde{W}B} \right), \\ g_{4}^{gg} &= -2 \frac{v^{2}}{\Lambda^{2}} \left(c_{W}^{2} C_{H\tilde{B}} + s_{w}^{2} C_{H\tilde{W}} - s_{w} c_{w} C_{H\tilde{W}B} \right), \\ g_{4}^{gg} &= -2 \frac{v^{2}}{\Lambda^{2}} \left(c_{W}^{2} C_{H\tilde{B}} + s_{w}^{2} C_{H\tilde{W}} - s_{w} c_{w} C_{H\tilde{W}B} \right), \\ g_{4}^{gg} &= -2 \frac{v^{2}}{\Lambda^{2}} \left(c_{W}^{2} C_{H\tilde{B}} + s_{w}^{2} C_{H\tilde{W}} - s_{w} c_{w} C_{H\tilde{W}B} \right), \\ g_{4}^{gg} &= -2 \frac{v^{2}}{\Lambda^{2}} \left(c_{W}^{2} C_{H\tilde{B}} + s_{w}^{2} C_{H\tilde{W}} - s_{w} c_{w} C_{H\tilde{W}B} \right), \\ g_{4}^{gg} &= -2 \frac{v^{2}}{\Lambda^{2}} \left(c_{W}^{2} C_{H\tilde{B}} + s_{w}^{2} C_{H\tilde{W}} - s_{w} c_{w} C_{H\tilde{W}B} \right), \\ g_{4}^{gg} &= -2 \frac$$

where Λ is the scale of new physics, which we set to $\Lambda=1~{\rm TeV}$ as a convention, and δg_1^{ZZ} is the correction to the SM value of $g_1^{ZZ}=2$. According to Eq. (5), $\delta g_1^{WW}=\delta g_1^{ZZ}$, and the other dependent amplitude coefficients can be derived from Eqs. (6)–(9).

A numerical example of the relationship between the $C_{HX} = 1$ contribution of a single operator in the Warsaw basis and the couplings in the mass-eigenstate amplitude in Eq. (1) is shown in Table I, which corresponds to the reverse of Eq. (10).

B. Application to the VBF, VH, and $H \rightarrow VV$ processes

One of the new features in this paper, compared to the earlier work, is the study of the $g_2^{Z\gamma}$, $g_2^{\gamma\gamma}$, $g_4^{Z\gamma}$, and $g_4^{\gamma\gamma}$ anomalous couplings in electroweak production of the H

boson. Their effect in the $H \to 4\ell$ process was studied with LHC data [48] and with phenomenological tools [25,35]. In the following we reexamine the $H \to 4\ell$ decay and investigate the VBF and VH processes. In the case of VH production, we consider three final states $Z(\to f\bar{f})H$, $\gamma^*(\to f\bar{f})H$, and γH , and both $q\bar{q}$ or gg production channels, as all are affected by the HVV couplings of our interest. While the gluon fusion process formally appears at higher order in QCD, the large gluon-parton luminosity at the LHC makes this channel interesting to examine.

In this study, we only examine the operators affecting the H boson interactions in Table I and study their effect on the HVV couplings. Other operators, such as HZff contact terms for example, are included in the JHUGen framework, but they are not the primary interest in this study because their existence would become evident in resonance searches and in electroweak measurements, without the need for H boson production. Moreover, such contact terms are equivalent to the combination of the κ_1^{ZZ} and $\kappa_2^{Z\gamma}$ couplings if flavor universality is assumed [45]. Not only HVV interactions may be affected by the above operators in the processes under study. For example, the C_{HWB} operator also affects the Zff couplings. However, these Zff couplings should be well constrained in electroweak measurements. For this reason, should one of the considered operators affect the Zff interactions, we assume some other operators not affecting the direct H boson interactions must also contribute to bring the Zff couplings to the SM values.

Numerical results of the relative contributions of operators to the $H \to VV \to 4\ell$, VBF, $q\bar{q}$ or $gg \to V(\to \ell^+\ell^-)H$, and γH processes are shown in Appendix A. The general observations from Tables IV–VI is that the relative importance of the $g_2^{Z\gamma}$, $g_2^{\gamma\gamma}$, $g_4^{Z\gamma}$, and $g_4^{\gamma\gamma}$ couplings changes between the processes. Taking the example of the C_{HWB} operator, these couplings lead to an overwhelming contribution in the $H \to 4\ell$ process. However, their contribution in the VBF and VH processes is not significant and is especially tiny in the case of the VH process.

TABLE I. The values of the couplings in the mass-eigenstate amplitude in Eq. (1) corresponding to the $C_{HX}=1$ contribution of a single operator in the Warsaw basis with $\Lambda=1$ TeV. The relationship corresponds to the reverse of Eq. (10). When quoting the $\kappa_2^{Z\gamma}$ and $\kappa_1^{ZZ}=\kappa_2^{ZZ}$ values, we set $\Lambda_1^{Z\gamma}=\Lambda_1^{ZZ}=100$ GeV in Eq. (1).

	$\delta g_1^{ZZ} = \delta g_1^{WW}$	κ_1^{ZZ}	g_2^{ZZ}	$g_2^{Z\gamma}$	$g_2^{\gamma\gamma}$	g_4^{ZZ}	$g_4^{Z\gamma}$	$g_4^{\gamma\gamma}$	$\kappa_2^{Z\gamma}$	κ_1^{WW}	g_2^{WW}	g_4^{WW}
$C_{H\square}$	0.1213	0	0	0	0	0	0	0	0	0	0	0
C_{HD}	0.2679	-0.0831	0	0	0	0	0	0	-0.1320	-0.1560	0	0
C_{HW}	0	0	-0.0929	-0.0513	-0.0283	0	0	0	0	0	-0.1212	0
C_{HWB}	0.1529	-0.0613	-0.0513	0.0323	0.0513	0	0	0	0.1763	0.0360	0	0
C_{HB}	0	0	-0.0283	0.0513	-0.0929	0	0	0	0	0	0	0
$C_{H ilde{W}}$	0	0	0	0	0	-0.0929	-0.0513	-0.0283	0	0	0	-0.1212
$C_{H ilde{W}B}$	0	0	0	0	0	-0.0513	0.0323	0.0513	0	0	0	0
$C_{H ilde{B}}$	0	0	0	0	0	-0.0283	0.0513	-0.0929	0	0	0	0

These features will affect our ability to use different processes to constrain anomalous couplings with photons. We note that the VH process with $V \to \ell^+ \ell^-$ includes both ZH and γ^*H production mechanisms, where γ^* leads to low- q^2 contributions in the $m_{\ell\ell}$ invariant mass, which can be observed in kinematic distributions.

The $gg \to ZH$ process has been shown to have no contributions of the two anomalous HVV tensor structures appearing in Eq. (1) in the triangular loop diagram [45]. Therefore, only the SM-like tensor structure with the g_1 and κ_1^{ZZ} couplings contributes to this diagram, as shown in Table VII. The off-shell photon does not couple to the triangular fermion loop either [45], and, therefore, the $\kappa_2^{Z\gamma}$ coupling does not contribute. The box diagram is sensitive to the fermion couplings of the H boson, which we do not vary in this study of anomalous HVV interactions. As the result, the $gg \to ZH$ process features a rather limited set of EFT operators and we will not study this process in more detail in this paper, leaving further details to Ref. [45].

The γH production process has been largely neglected in analysis of LHC data. However, this process was used in the search for the H boson with anomalous couplings in e^+e^- production prior to the H boson discovery [82] and proposed in application to CP-even EFT operator constraints at the LHC [83,84]. From Table VIII, it is evident that only the $g_2^{Z\gamma}$, $g_2^{\gamma\gamma}$, $g_4^{Z\gamma}$, and $g_4^{\gamma\gamma}$ couplings contribute, and this channel does not receive tree-level SM contributions. Because the photon is on shell, it does not receive contributions from $\kappa_2^{Z\gamma}$ either. This process is generated by the dimension-six operators squared in the EFT expansion in combination with the EW loops generated by the SM particles. As an approximation to the SM production cross section, we use the calculation with the $g_2^{\rm Z\gamma,SM}$ and $g_2^{\gamma\gamma,\text{SM}}$ values calculated in Sec. V. These pointlike couplings reproduce the SM decay width of the processes $H \rightarrow$ $Z\gamma$ and $\gamma\gamma$, respectively. Due to the off-shell $V=Z/\gamma^*$ in the process $q\bar{q} \to V \to \gamma H$, these pointlike couplings are not expected to reproduce the full EW loop calculation in the SM, but they are expected to provide a good estimate, which we use as $\sigma_{\rm SM}^{\gamma H}$ in Table VIII. The γH process may be of particular interest in isolating the CP-odd couplings $g_4^{Z\gamma}$ and $g_4^{\gamma\gamma}$ in combination with *CP*-even couplings $g_2^{Z\gamma}$ and $g_2^{\gamma\gamma}$, which is complementary to the $H \to Z\gamma$ and $\gamma\gamma$ decays.

C. Kinematic distributions with EFT effects

The kinematic effects in the $H \rightarrow VV$, VBF, and VH processes can typically be described with five angular observables and two invariant masses, or q_i^2 of the two vector bosons, as illustrated in Fig. 1 [19,28,45]. The distributions of two of these angles, θ^* and Φ_1 , are random

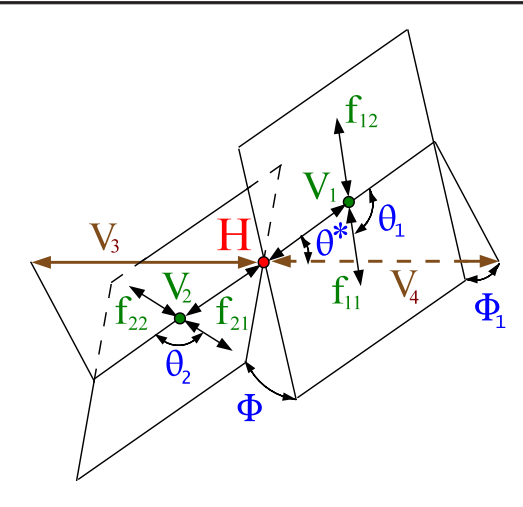


FIG. 1. Three kinematic topologies of the H boson production and decay [45]: vector boson fusion $q_{12}q_{22} \rightarrow q_{11}q_{21}(V_1V_2 \rightarrow H \rightarrow V_3V_4)$, VH production $q_{11}q_{12} \rightarrow V_1 \rightarrow V_2(H \rightarrow V_3V_4)$, and four-fermion decay $V_3V_4 \rightarrow H \rightarrow V_1V_2 \rightarrow 4f$.

for a spin-zero H boson, but are less trivial for a higher-spin resonance or nonresonant production. In the following, we disentangle the relative contributions of the ZZ, WW, $Z\gamma$, and $\gamma\gamma$ intermediate vector-boson states to simulation with a given operator in the Warsaw basis. Such a decomposition reveals interesting kinematic effects and also allows us to validate the tools used for simulation of EFT effects and match their conventions.

We use the JHUGen program to generate several models which allow us to visualize the relative contributions of the mass eigenstates of the vector bosons. We also model the inclusive kinematic distributions with the SMEFTsim program [85] using MadGraph5 simulation [86]. Once the sign conventions are matched, as discussed in Sec. II, we find good agreement. A similar comparison with SM couplings using the PROPHECY4F [87] and HAWK [88] generators is shown in Sec. V. Throughout this paper and unless otherwise noted, the calculations are performed at leading order (LO) in QCD and EW, with the \overline{MS} -mass for the top quark $m_t = 162.7$ GeV, the on-shell mass for the bottom quark $m_b = 4.18 \text{ GeV}$, QCD scale $\mu = M_H/2$, $\alpha_s = 0.1188$, $\alpha = 1/128$, $s_w^2 = 0.23119$, $G_F = 1.16639 \times$ 10⁻⁵ GeV⁻² [89], and the NNPDF 3.0 parton distribution functions [90].

In the $H \to 4\ell$ and VH processes, we require $m_{\ell\ell} > 1$ GeV. In the VBF process, we apply the selection requirements $m_{jj} > 300$ GeV, $p_T^{\rm jet} > 1$ GeV, $|\eta^{\rm jet}| < 5$, $\Delta \eta_{jj} > 1$, $\Delta R_{jj} > 0.3$, $\sqrt{q_V^2} > 15$ GeV. In the $H \to 4\ell$ decay, we model the $C_{HWB} = 1$ contribution to the SM, as shown in Fig. 2 with cross section decomposition presented in Table IV. In VBF or VH, we model the $C_{H\bar{W}B} = 10$ or $C_{HB} = 100$ contribution to the SM, as shown in Fig. 3 or Fig. 4, with the cross section decomposition presented in

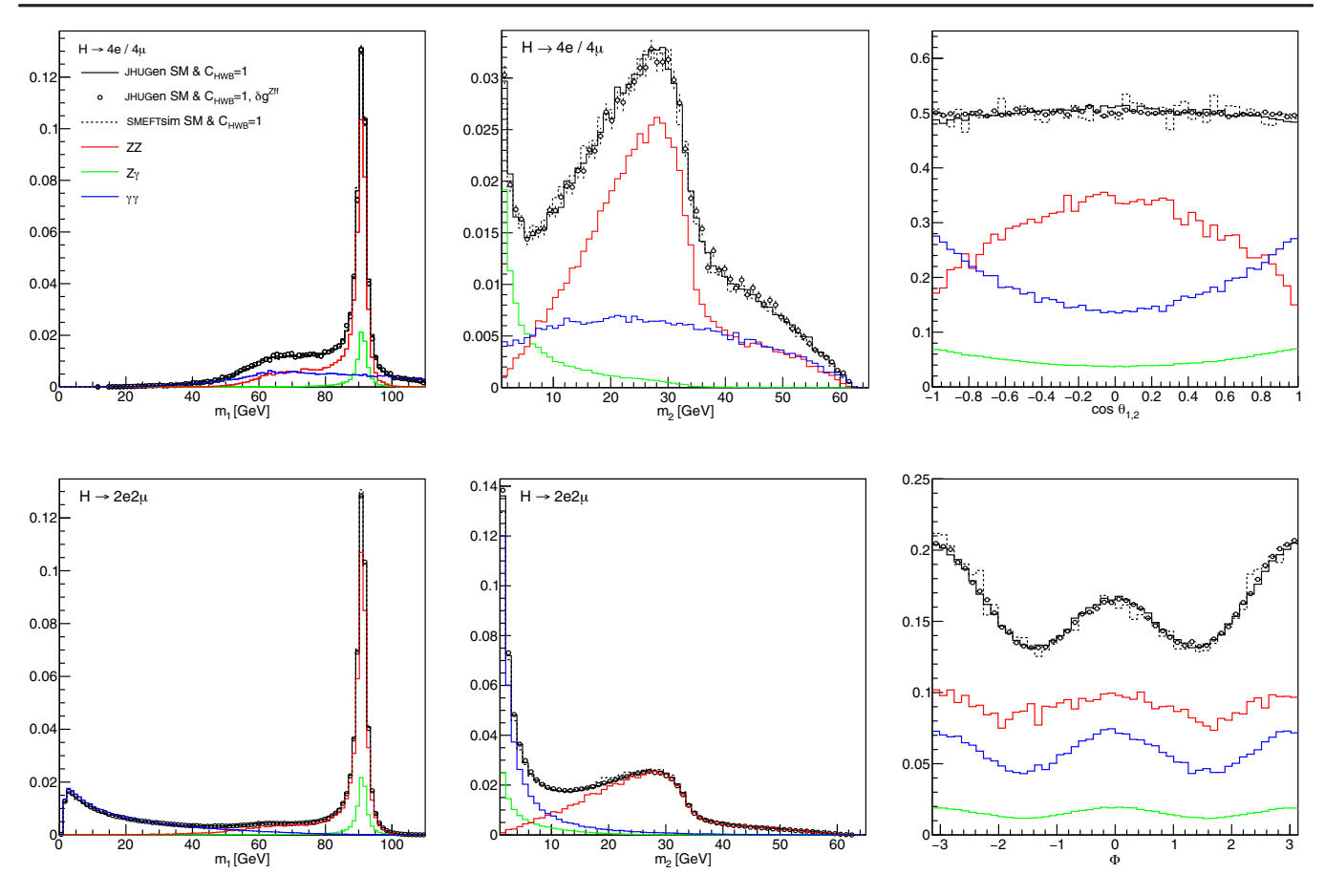


FIG. 2. Distribution of the larger (left) and smaller (middle) dilepton invariant mass in the $H \to 4e/4\mu$ (top) and $H \to 2e2\mu$ (bottom) decay. Also shown are the $\cos\theta_{1,2}$ (top right) and Φ (bottom right) distributions in the $H \to 2e2\mu$ decay. Distributions are generated with JHUGen for $C_{HWB}=1$, with the three contributions due to the HZZ (red), $HZ\gamma$ (green), and $H\gamma\gamma$ (blue) couplings shown separately. The JHUGen distributions are shown without (solid) and with (points) corrections to the Zff couplings, indicated with δg^{Zff} . The comparison to SMEFTsim modeling (dashed) is also shown.

Table V or Table VI. The size of anomalous contributions is chosen to be large compared to SM for visibility of their contributions.

In the $H \to 4\ell$ process, the larger and the smaller invariant masses of the dilepton pairs m_1 and m_2 are the two observables representing q_1^2 and q_2^2 . In Fig. 2, there are clear peaks towards $m_2 \rightarrow 0$ in the case of couplings with photons, $HZ\gamma$ and $H\gamma\gamma$, a feature to which we will return in Secs. IV, V, and VI. In the case of $H\gamma\gamma$, this extends to $m_1 \to 0$ as well. Modeling such contributions becomes essential, and we will discuss extensions of such modeling to $m_{\ell\ell} < 1$ GeV later. Moreover, in analysis of experimental data, detector effects change significantly for either γ^* or Z intermediate states, and dedicated simulation of such effects with the full detector modeling becomes important. In Fig. 2, the m_1 and m_2 distributions are shown separately in the $H \to 4e/4\mu$ and $H \to 2e2\mu$ decays. The interference of two diagrams with permutation of identical leptons in the case of $H \rightarrow 4e/4\mu$ leads to suppression of the peaks at $m_1 \to 0$ and $m_2 \to 0$ in the case of $H\gamma\gamma$. This feature becomes important in analysis of the $H\gamma\gamma$ couplings.

Since Zff couplings have been constrained with precision EW data, we do not allow their change in these studies and assume that modification of other operators, not contributing to the H boson couplings, can compensate any possible shift of the Zff couplings due to C_{HWB} . However, in Fig. 2 we also show distributions with modification of the Zff couplings, indicated with δg^{Zff} . Corrections to the multidimensional angular distributions are expected due to nonzero values of the R_i and A_f parameters discussed in Refs. [19,23,28]. These corrections are visible in the projection on the Φ observable in Fig. 2, but are very small for any practical purpose with the typical values of C_{HWB} in the present studies. These corrections become sizable with larger values of C_{HWB} .

In the VBF process, we can calculate the $q_{1,2}^{\rm VBF}=\sqrt{-q_{1,2}^2}$ values using the momenta of the fully reconstructed H boson and two jets and using the direction

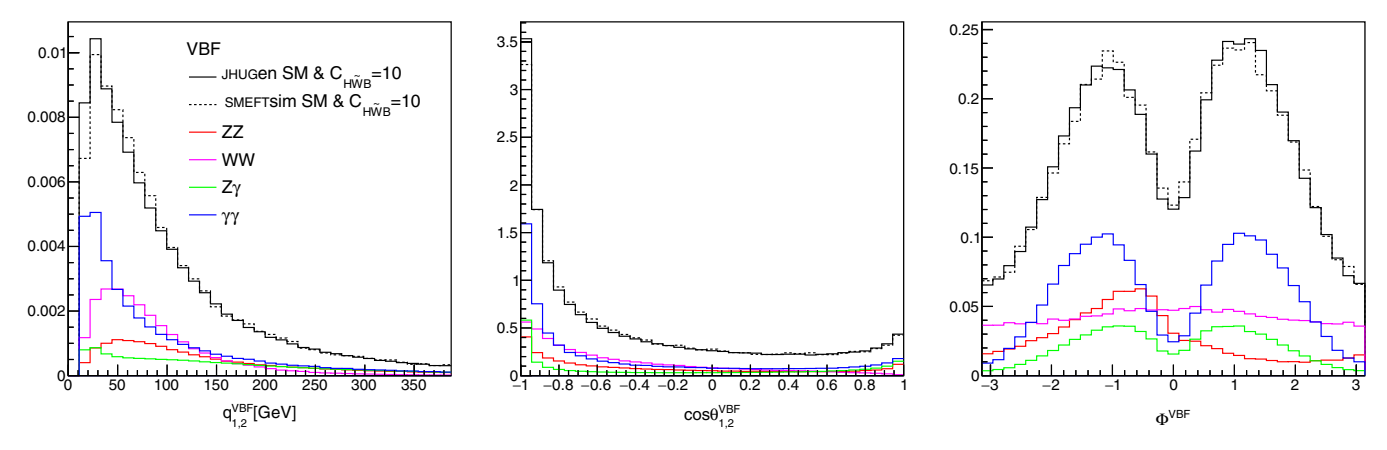


FIG. 3. Distribution of $\sqrt{-q_{1,2}^2}$ (left), $\cos\theta_{1,2}^{\rm VBF}$ (middle), and $\Phi^{\rm VBF}$ (right) for the intermediate vector boson in the VBF process generated with JHUGen for the $C_{H\tilde{W}B}=10$ with three contributions due to the HZZ (red), HWW (magenta), $HZ\gamma$ (green), and $H\gamma\gamma$ (blue) couplings shown separately. The comparison to SMEFTsim modeling (dashed) is also shown.

of incoming partons along the proton beams. In Fig. 3, there is a clear preference of lower $q_{1,2}^{\rm VBF}$ values in the case of couplings with photons. There is a strong correlation between the $q_{1,2}^{\rm VBF}$ values and the transverse momentum p_T of the jets, which leads to different detector effects. We note the asymmetric distribution of the $\Phi^{\rm VBF}$ angle in Fig. 3, which is most visible in the HZZ process but can also be seen in the combined distribution. This happens due to interference of the CP-even SM amplitude and CP-odd $C_{H\tilde{W}B}=10$ contributions.

In the VH process, q_1^2 and q_2^2 represent the VH and the $V \to \ell^+ \ell^-$ invariant masses, respectively. There are particularly dramatic effects in the $m_{\ell\ell}$ distribution, shown in Fig. 4, where the virtual photon γ^* results in the low-mass enhancement, as opposed to the peak at m_Z . A dedicated analysis of the small invariant masses in the $\gamma^* H$ production may be needed for effective EFT analysis of the process.

Another approach to study anomalous H boson couplings involving photons is analysis of the γH process, which distinguishing feature is a high-momentum on-shell photon associated with the H boson. In the LO topology, where the γH system has no transverse boost, the transverse momentum of either photon γ or the H boson is a dependent observable and the three primary measurements are the rapidity y and the invariant mass $m_{\gamma H}$ of the $m_{\gamma H}$ system, and the angle θ_1 formed by the outgoing photon with respect to the direction of incoming quark in the γH rest frame. This angle is also defined in Fig. 1, where $V_2 = \gamma$ and which does not have a subsequent decay. While it is not possible to distinguish the incoming quark and antiquark on an event-by-event basis, on average the boost direction of the γH provides the preferred direction of the quark, and we use this to define θ_1 . However, determination of the $\cos \theta_1$ sign becomes important only in the special case of the forward-backward asymmetry discussed below. The ability to determine the $\cos \theta_1$ sign is a function of y and has been discussed earlier [45,91].

In Fig. 5 the $m_{\gamma H}$ and $\cos\theta_1^{VH}$ distributions are shown for the $g_2^{Z\gamma}$, $g_2^{\gamma\gamma}$, $g_4^{Z\gamma}$, or $g_4^{\gamma\gamma}$ anomalous couplings, and for the mixture of $g_2^{Z\gamma}$ and $g_4^{Z\gamma}$ contributions with a complex phase of $g_4^{Z\gamma}$. The $m_{\gamma H}$ distributions differ somewhat between the $HZ\gamma$ and $H\gamma\gamma$ couplings, due to the difference between the intermediate Z^* and γ^* . The $\cos\theta_1^{VH}$ distributions follow the $(1+\cos^2\theta_1)$ expectation for all real couplings. This expectation can be traced back to Eq. (A2) in Ref. [28], where $A_{00}=0$, which must be averaged over Φ and $\cos\theta_2$. The situation becomes similar to the angular distribution in the $H\to Z\gamma$ decay, described with the same angular parametrization, as shown in Fig. 15 of Ref. [28], and where the forward-backward asymmetry may be generated with the mixture of CP-odd and CP-even couplings and in the presence of a complex phase.

The size of the forward-backward asymmetry is proportional to the A_f parameter defined in Ref. [28] for Zff couplings, which is 0.15 for the lepton couplings, but is as large as 0.67 and 0.94 for the up- and down-type quarks. Therefore, despite the sizable dilution in the measurement of the $\cos\theta_1$ sign, the forward-backward asymmetry is strongly pronounced in Fig. 5 and could be measured in experiment once γH production is observed. The A_f parameter is zero for the photon couplings γff , and such an effect is not possible in the mixture of couplings involving $g_2^{\gamma\gamma}$ and $g_4^{\gamma\gamma}$. Since nontrivial forward-backward asymmetry appears only in the special case of complex couplings, we do not consider this asymmetry further in this work, but we point out that such a study is, in principle, possible.

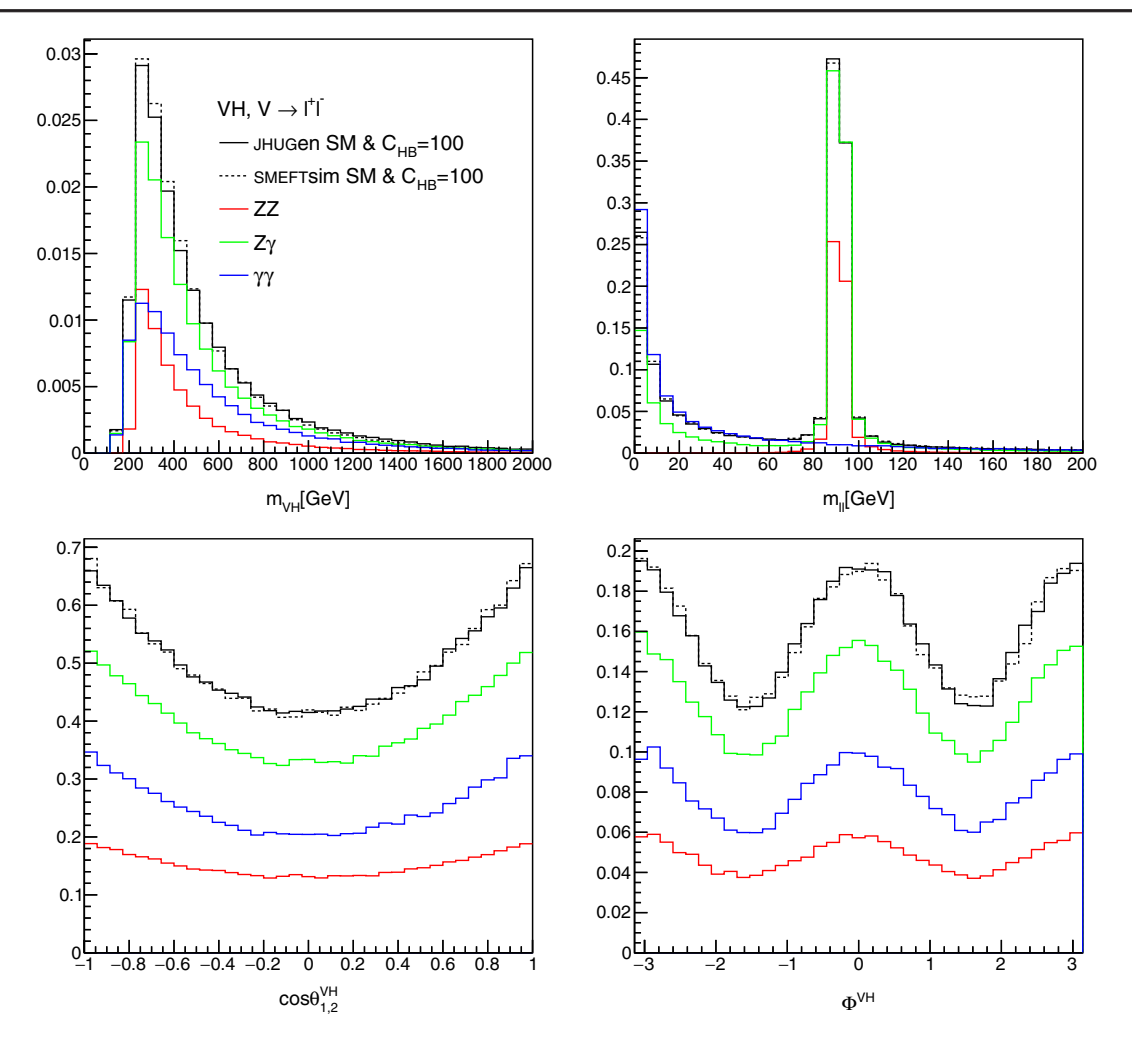


FIG. 4. Distribution of the m_{VH} (top left) and $m_{\ell\ell}$ (top right) invariant masses, $\cos\theta_{1,2}^{VH}$ (bottom left), and Φ^{VH} (bottom right) in the $q\bar{q} \to VH \to \ell\ell H$ process generated with JHUGen for the $C_{HB}=100$ with three contributions due to the HZZ (red), $HZ\gamma$ (green), and $H\gamma\gamma$ (blue) couplings shown separately. The comparison to SMEFTsim modeling (dashed) is also shown.

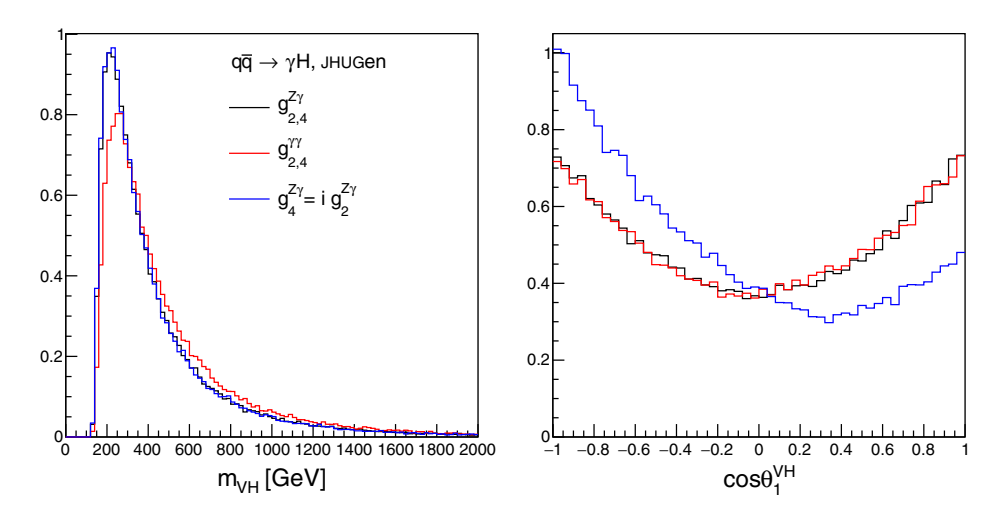


FIG. 5. Distribution of $m_{\gamma H}$ (left) and $\cos\theta_1^{VH}$ (right) in the $q\bar{q}\to\gamma H$ process generated with JHUGen with the $g_2^{Z\gamma}$, $g_2^{\gamma\gamma}$, $g_4^{Z\gamma}$, or $g_4^{\gamma\gamma}$ anomalous couplings. Distributions for individual couplings are shown in black $(HZ\gamma)$ and red $(H\gamma\gamma)$, and the mixture of $g_2^{Z\gamma}$ and $g_4^{Z\gamma}$ couplings with the complex ratio is shown in blue.

IV. PARAMETRIZATION OF CROSS SECTIONS

In this section we discuss the relationship between the coupling constants and the cross section of a process involving the H boson. In Ref. [45], we calculated the scaling factors for the partial decay widths in the nine dominant H boson decay modes as a function of anomalous couplings a_i , including the $H \to gg$, $\gamma\gamma$, and $Z\gamma$ decays, by resolving the loop contributions. However, we omitted pointlike contributions such as $g_{2,4}^{\gamma\gamma}$ and $g_{2,4}^{Z\gamma}$ due to their relatively lower importance in the VBF, VH, and $H \rightarrow 4f$ processes. Such couplings could be generated by a heavy quark Q with mass $m_Q \gg M_H$. We assume that its couplings to the H boson are κ_Q and $\tilde{\kappa}_Q$, the number of colors N_c , the electric charge Q, and the weak isospin projection T^{3L} . This special model allows us to derive the pointlike interactions and relate those to the partial decay widths. While derivation applies to this special case, the final expression in terms of the $g_{2,4}^{gg}$, $g_{2,4}^{\gamma\gamma}$, and $g_{2,4}^{Z\gamma}$ couplings becomes generic and remains valid for any new physics in the loop, generated by any combination of heavy fermions or bosons. Therefore, the resulting expressions are applicable to the general treatment of these loops in the EFT approach.

First, we recall that in the narrow-width approximation for on-shell H boson production and decay, the cross section can be expressed as

$$\sigma(i \to H \to f) \propto \frac{\left(\sum \alpha_{jk}^{(i)} a_j a_k\right) \left(\sum \alpha_{lm}^{(f)} a_l a_m\right)}{\Gamma_{\text{tot}}}, \quad (11)$$

where the total width $\Gamma_{tot} = \Gamma_{known} + \Gamma_{other}$ representing decays to known particles and other unknown final states, either invisible or undetected in experiment. In the following we will focus on decay to the known SM particles which can be expressed as a sum of all partial decay widths as

$$\Gamma_{\text{known}} = \Gamma_{\text{tot}}^{\text{SM}} \times \sum_{f} \left(\frac{\Gamma_{f}^{\text{SM}}}{\Gamma_{\text{tot}}^{\text{SM}}} \times \frac{\Gamma_{f}}{\Gamma_{f}^{\text{SM}}} \right) = \sum_{f} \Gamma_{f}^{\text{SM}} R_{f},$$
(12)

where R_f is the scaling factor as function of the coupling constants a_i , and Γ_f^{SM} is the SM value of the partial decay width in the final state f.

In the following, we rely on JHUGen framework implementation, discussed in Sec. III and Ref. [45], to derive the loop contributions of the SM particles and the heavy quark Q to the scaling factor $R_{\rm gg}$, for both CP-even and CP-odd couplings. The CP-even coupling contributions of the quarks and W boson to $R_{\gamma\gamma}$ and $R_{Z\gamma}$ are derived with HDECAY [92]. The CP-odd contributions to $R_{\gamma\gamma}$ are calculated with the JHUGen framework in a manner analogous to

 $R_{\rm gg}$. The *CP*-odd contributions to $R_{Z\gamma}$ are calculated using CHDECAY [93].

The ratio of the decay width to the SM expectation in the $H \rightarrow gg$ process [45] is found to be

$$R_{gg} = 1.1068\kappa_t^2 + 0.0082\kappa_b^2 - 0.1150\kappa_t \kappa_b + 2.5717\tilde{\kappa}_t^2 + 0.0091\tilde{\kappa}_b^2 - 0.1982\tilde{\kappa}_t \tilde{\kappa}_b + 1.0298(N_c/3)^2\kappa_Q^2 + 2.1357(N_c/3)\kappa_Q \kappa_t - 0.1109(N_c/3)\kappa_Q \kappa_b + 2.3170(N_c/3)^2\tilde{\kappa}_Q^2 + 4.8821(N_c/3)\tilde{\kappa}_Q \tilde{\kappa}_t - 0.1880(N_c/3)\tilde{\kappa}_Q \tilde{\kappa}_b.$$
(13)

The κ_Q and $\tilde{\kappa}_Q$ couplings are connected to the $g_2^{\rm gg}$ and $g_4^{\rm gg}$ pointlike interactions introduced in Eq. (1) through

$$g_2^{\text{gg},\mathcal{Q}} = -\alpha_s N_c \kappa_{\mathcal{Q}}/(18\pi), \quad g_4^{\text{gg},\mathcal{Q}} = -\alpha_s N_c \tilde{\kappa}_{\mathcal{Q}}/(12\pi). \quad (14)$$

One can rewrite Eq. (13) in terms of the $g_2^{\rm gg}$ and $g_4^{\rm gg}$ couplings in place of $N_c\kappa_{\mathcal Q}$ and $N_c\tilde\kappa_{\mathcal Q}$ by substituting Eq. (14). Even though Eq. (14) is derived in the special case of a heavy quark, the resulting expression of $R_{\rm gg}$ as a function of $g_2^{\rm gg}$ and $g_4^{\rm gg}$ and other terms is valid for any heavy particles in the loop that generate these pointlike interactions.

The latter observation allows us to obtain the value of the effective $g_2^{\rm gg}$ coupling which leads to the SM cross section in the gluons fusion process. By setting all couplings, other than $g_2^{\rm gg}$, to zero and $R_{\rm gg}=1$ in Eq. (13), we obtain

$$g_2^{\text{gg,SM}} = -0.00621. \tag{15}$$

The $g_2^{\rm gg,SM}$ value differs by only 1.5% from the value that one would obtain in the heavy top mass limit by setting $\kappa_{\mathcal{Q}}=1$ and $N_c=3$ in Eq. (14), and the sign follows the prediction in this limit.

An approximate way to express Eq. (13) with the pointlike interactions only in the case of SM couplings of fermions $\kappa_t = \kappa_b = 1$ and $\tilde{\kappa}_t = \tilde{\kappa}_b = 0$ would be to substitute the top and bottom quark contributions with an effective coupling $g_2^{\rm gg,SM}$ from Eq. (15), substitute $\kappa_{\mathcal{Q}}$ and $\tilde{\kappa}_{\mathcal{Q}}$ for $g_2^{\rm gg}$ and $g_4^{\rm gg}$, and obtain

$$R_{\rm gg} \simeq \frac{1}{(g_2^{\rm gg,SM})^2} \left[\left(g_2^{\rm gg,SM} + g_2^{\rm gg} \right)^2 + \left(g_4^{\rm gg} \right)^2 \right].$$
 (16)

For the $H \to \gamma \gamma$ final states, we include the W boson in addition to the top, bottom, and heavy $\mathcal Q$ quarks in the loop and obtain²

²Due to updated EW parameters, there is a small change in the numerical values of coefficients in Eqs. (17) and (26) that are in common with Ref. [45].

$$R_{\gamma\gamma} = 1.60932 \left(\frac{g_1^{WW}}{2}\right)^2 - 0.69064 \left(\frac{g_1^{WW}}{2}\right) \kappa_t + 0.00912 \left(\frac{g_1^{WW}}{2}\right) \kappa_b - 0.49725 \left(\frac{g_1^{WW}}{2}\right) (N_c Q^2 \kappa_Q)$$

$$+ 0.07404 \kappa_t^2 + 0.00002 \kappa_b^2 - 0.00186 \kappa_t \kappa_b + 0.03841 (N_c Q^2 \kappa_Q)^2 + 0.10666 \kappa_t (N_c Q^2 \kappa_Q)$$

$$- 0.00136 \kappa_b (N_c Q^2 \kappa_Q) + 0.20533 \tilde{\kappa}_t^2 + 0.00006 \tilde{\kappa}_b^2 - 0.00300 \tilde{\kappa}_t \tilde{\kappa}_b + 0.10252 (N_c Q^2 \tilde{\kappa}_Q)^2$$

$$+ 0.29018 \tilde{\kappa}_t (N_c Q^2 \tilde{\kappa}_Q) - 0.00202 \tilde{\kappa}_b (N_c Q^2 \tilde{\kappa}_Q).$$

$$(17)$$

For the contribution of a heavy quark in the loop we find

$$g_2^{\gamma\gamma,Q} = -\frac{\alpha}{3\pi} N_c Q^2 \kappa_Q, \quad g_4^{\gamma\gamma,Q} = -\frac{\alpha}{2\pi} N_c Q^2 \tilde{\kappa}_Q.$$
 (18)

Following the idea described above for $R_{\rm gg}$, one can rewrite Eq. (17) in terms of the $g_2^{\gamma\gamma}$ and $g_4^{\gamma\gamma}$ couplings in place of $N_c Q^2 \kappa_Q$ and $N_c Q^2 \tilde{\kappa}_Q$ by substituting Eq. (18). The final expression of $R_{\gamma\gamma}$ as a function of $g_2^{\gamma\gamma}$ and $g_4^{\gamma\gamma}$ and other terms is again valid for any heavy particles in the loop, fermions or bosons, that generate these pointlike interactions. By setting all couplings other than $g_2^{\gamma\gamma}$ to zero and $R_{\gamma\gamma}=1$ in Eq. (17), we obtain the effective coupling which leads to the SM cross section

$$g_2^{\gamma\gamma,\text{SM}} = 0.00423.$$
 (19)

The $g_2^{\gamma\gamma, \rm SM}$ value differs slightly from 0.00400 obtained from the general expression of the SM loops derived from Refs. [94,95] and shown in Eq. (20). The difference could be explained by the higher-order effects incorporated in Eq. (17) and the fact that in our approach we match the SM rate $R_{\gamma\gamma}=1$. The sign in Eq. (19) follows Eq. (20).

$$g_2^{\gamma\gamma} = \left(-\frac{\alpha}{4\pi}\right) \left[\left(\frac{g_1^{WW}}{2}\right) \times A_1^{\gamma\gamma}(\tau_W) + \kappa_t N_c Q_t^2 \times A_{1/2}^{\gamma\gamma}(\tau_t) \right]$$
$$= 0.00516 \left(\frac{g_1^{WW}}{2}\right) - 0.00116\kappa_t, \tag{20}$$

where the one-loop functions are given by

$$A_1^{\gamma\gamma}(\tau_W) = \begin{cases} -8.32 & \text{for } \tau_W = M_W^2 / M_H^2 \\ -7 & \text{for } \tau_W \to \infty, \end{cases}$$
 (21)

and

$$A_{1/2}^{\gamma\gamma}(\tau_t) = \begin{cases} +1.38 & \text{for } \tau_t = m_t^2 / M_H^2 \\ +4/3 & \text{for } \tau_t \to \infty \end{cases}$$
 (22)

An approximate way to express Eq. (17) with pointlike interactions only would be to follow the idea used to create Eq. (16) and substitute the SM couplings with $g_2^{\gamma\gamma, \text{SM}}$ from Eq. (19), substitute $\kappa_{\mathcal{Q}}$ and $\tilde{\kappa}_{\mathcal{Q}}$ for $g_2^{\gamma\gamma}$ and $g_4^{\gamma\gamma}$, and obtain

$$R_{\gamma\gamma} \simeq \frac{1}{(g_2^{\gamma\gamma,\text{SM}})^2} [(g_2^{\gamma\gamma,\text{SM}} + g_2^{\gamma\gamma})^2 + (g_4^{\gamma\gamma})^2].$$
 (23)

For the $H \to Z\gamma$ final states, for the coupling of the heavy Q quark to the Z boson, we introduce the following parameter

$$\mathcal{R}_{\mathcal{Q}} = Q \frac{T_{\mathcal{Q}}^{3L} - 2s_w^2 Q}{s_w c_w},\tag{24}$$

which corresponds to the following values for the SM parameters of the top $(T_t^{3L}=+1/2,\ Q_t=+2/3)$ and bottom $(T_b^{3L}=-1/2,\ Q_b=-1/3)$ quarks

$$\mathcal{R}_t = 0.3032, \quad \mathcal{R}_b = 0.2735.$$
 (25)

We obtain

$$R_{Z\gamma} = 1.11965 \left(\frac{g_1^{WW}}{2}\right)^2 - 0.12652 \left(\frac{g_1^{WW}}{2}\right) \kappa_t + 0.00348 \left(\frac{g_1^{WW}}{2}\right) \kappa_b - 0.13021 \left(\frac{g_1^{WW}}{2}\right) (N_c \mathcal{R}_{\mathcal{Q}} \kappa_{\mathcal{Q}})$$

$$+ 0.00357 \kappa_t^2 + 0.000003 \kappa_b^2 - 0.00018 \kappa_t \kappa_b + 0.00377 (N_c \mathcal{R}_{\mathcal{Q}} \kappa_{\mathcal{Q}})^2 + 0.00734 \kappa_t (N_c \mathcal{R}_{\mathcal{Q}} \kappa_{\mathcal{Q}})$$

$$- 0.00019 \kappa_b (N_c \mathcal{R}_{\mathcal{Q}} \kappa_{\mathcal{Q}}) + 0.00849 \tilde{\kappa}_t^2 + 0.000004 \tilde{\kappa}_b^2 - 0.00025 \tilde{\kappa}_t \tilde{\kappa}_b + 0.00883 (N_c \mathcal{R}_{\mathcal{Q}} \tilde{\kappa}_{\mathcal{Q}})^2$$

$$+ 0.01723 \tilde{\kappa}_t (N_c \mathcal{R}_{\mathcal{Q}} \tilde{\kappa}_{\mathcal{Q}}) - 0.00024 \tilde{\kappa}_b (N_c \mathcal{R}_{\mathcal{Q}} \tilde{\kappa}_{\mathcal{Q}}).$$

$$(26)$$

For the contribution of heavy fourth-generation quarks in the loop we find

$$g_2^{Z\gamma,Q} = -\frac{\alpha}{6\pi} N_c \mathcal{R}_Q \kappa_Q, \quad g_4^{Z\gamma,Q} = -\frac{\alpha}{4\pi} N_c \mathcal{R}_Q \tilde{\kappa}_Q.$$
 (27)

We note that the effective value of $g_2^{Z\gamma}$ for a heavy quark Q which reproduces the SM partial width, is

$$g_2^{\text{Z}\gamma,\text{SM}} = 0.00675.$$
 (28)

The $g_2^{Z\gamma, \rm SM}$ value differs slightly from 0.00724 obtained from the general expression of the SM loops derived from Refs. [94,95]³ and shown in Eq. (29). As before, the difference could be explained by the higher-order effects incorporated in Eq. (26) and the fact that in our approach we match the SM rate $R_{Z\gamma}=1$. The sign in Eq. (28) follows Eq. (29),

$$\begin{split} g_{2}^{Z\gamma} &= \frac{\alpha}{4\pi} \left[\left(\frac{g_{1}^{WW}}{2} \right) \frac{c_{w}}{s_{w}} \times A_{1}^{Z\gamma}(\tau_{W}) + \kappa_{t} N_{c} \mathcal{R}_{t} \times A_{1/2}^{Z\gamma}(\tau_{t}) \right] \\ &= 0.00747 \left(\frac{g_{1}^{WW}}{2} \right) - 0.00023 \kappa_{t}, \end{split} \tag{29}$$

where the one-loop functions are given by $A_1^{Z\gamma}(M_W^2/M_H^2)=6.58$ and $A_{1/2}^{Z\gamma}(m_t^2/M_H^2)=-0.35$.

An approximate way to express Eq. (26) with pointlike interactions only would be to substitute the SM contributions with an effective coupling $g_2^{Z\gamma, \text{SM}}$ from Eq. (28), substitute $\kappa_{\mathcal{O}}$ and $\tilde{\kappa}_{\mathcal{O}}$ for $g_2^{Z\gamma}$ and $g_2^{Z\gamma}$, and obtain

$$R_{Z\gamma} \simeq \frac{1}{\left(g_2^{Z\gamma,SM}\right)^2} \left[\left(g_2^{Z\gamma,SM} + g_2^{Z\gamma}\right)^2 + \left(g_4^{Z\gamma}\right)^2 \right].$$
 (30)

In the above calculation, the $H \to \gamma^* \gamma$ process is not included, for which the full-loop calculation with anomalous couplings is not available. For the $H \to ZZ/Z\gamma^*/\gamma^*\gamma^* \to$ four-fermion final state, the full one-loop calculation with anomalous couplings is not available either. The EW loop corrections under the SM assumption are discussed in Sec. V. A more careful treatment of the singularities appearing in the presence of anomalous couplings in both of the above cases is discussed in Sec. VI. For the leading tree-level contributions, we derived the $R_{ZZ/Z\gamma^*/\gamma^*\gamma^*}$ parametrization in Ref. [45], in which case we set $g_2^{Z\gamma} = g_4^{Z\gamma} = g_2^{\gamma\gamma} = g_4^{\gamma\gamma} = 0$ to avoid collinear singularities. In the following, we introduce these four couplings and avoid singularities in the $\gamma^* \to 2f$ transition with the finite fermion mass threshold $q^2 > (2m_f)^2$. We set $\Lambda_1^{Z\gamma} = \Lambda_1^{ZZ} = 100$ GeV in Eq. (1) and rely on the $\kappa_2^{Z\gamma}$ and $\kappa_1^{Z\gamma} = \kappa_2^{ZZ}$ parameters to express the scaling factor as $\Lambda_1^{Z\gamma} = \kappa_1^{ZZ} = \kappa_2^{ZZ}$ parameters to express the scaling factor

$$\begin{split} R_{ZZ/Z\gamma^*/\gamma^*\gamma^*} &= \left(\frac{g_1^{ZZ}}{2}\right)^2 + 0.17(\kappa_1^{ZZ})^2 + 0.09(g_2^{ZZ})^2 + 0.04(g_4^{ZZ})^2 + 0.10(\kappa_2^{Z\gamma})^2 + 79.95(g_2^{Z\gamma})^2 + 75.23(g_4^{Z\gamma})^2 \\ &+ 29.00(g_2^{\gamma\gamma})^2 + 29.47(g_4^{\gamma\gamma})^2 + 0.81\frac{g_1^{ZZ}}{2}\kappa_1^{ZZ} + 0.50\frac{g_1^{ZZ}}{2}g_2^{ZZ} + 0 \times \frac{g_1^{ZZ}}{2}g_4^{ZZ} - 0.19\frac{g_1^{ZZ}}{2}\kappa_2^{Z\gamma} - 1.56\frac{g_1^{ZZ}}{2}g_2^{Z\gamma} \\ &+ 0 \times \frac{g_1^{ZZ}}{2}g_4^{Z\gamma} + 0.06\frac{g_1^{ZZ}}{2}g_2^{\gamma\gamma} + 0 \times \frac{g_1^{ZZ}}{2}g_4^{\gamma\gamma} + 0.21\kappa_1^{ZZ}g_2^{ZZ} + 0 \times \kappa_1^{ZZ}g_4^{ZZ} - 0.07\kappa_1^{ZZ}\kappa_2^{Z\gamma} - 0.64\kappa_1^{ZZ}g_2^{Z\gamma} \\ &+ 0 \times \kappa_1^{ZZ}g_4^{Z\gamma} + 0.00\kappa_1^{ZZ}g_2^{\gamma\gamma} + 0 \times \kappa_1^{ZZ}g_4^{\gamma\gamma} + 0 \times g_2^{ZZ}g_4^{ZZ} - 0.05g_2^{ZZ}\kappa_2^{Z\gamma} - 0.51g_2^{ZZ}g_2^{Z\gamma} + 0 \times g_2^{ZZ}g_4^{Z\gamma} \\ &- 0.02g_2^{ZZ}g_2^{\gamma\gamma} + 0 \times g_2^{ZZ}g_4^{\gamma\gamma} + 0 \times g_4^{ZZ}\kappa_2^{Z\gamma} + 0 \times g_4^{ZZ}g_2^{Z\gamma} + 0.36g_4^{ZZ}g_4^{Z\gamma} + 0 \times g_4^{ZZ}g_2^{\gamma\gamma} - 0.57g_4^{ZZ}g_4^{\gamma\gamma} \\ &+ 1.80\kappa_2^{Z\gamma}g_2^{Z\gamma} + 0 \times \kappa_2^{Z\gamma}g_4^{Z\gamma} - 0.05\kappa_2^{Z\gamma}g_2^{\gamma\gamma} + 0 \times \kappa_2^{Z\gamma}g_4^{\gamma\gamma} + 0 \times g_2^{Z\gamma}g_4^{Z\gamma} - 1.84g_2^{Z\gamma}g_2^{\gamma\gamma} + 0 \times g_2^{Z\gamma}g_4^{\gamma\gamma} \\ &+ 0 \times g_4^{Z\gamma}g_2^{\gamma\gamma} - 2.09g_4^{Z\gamma}g_4^{\gamma\gamma} + 0 \times g_2^{\gamma\gamma}g_4^{\gamma\gamma} . \end{split}$$

Equation (31) covers all final states with $Z/\gamma^* \to q\bar{q}$ and $\ell^+\ell^-$ with quarks and charged leptons, while neutrinos are included with $Z \to \nu\bar{\nu}$. The treatment of $q\bar{q}$ hadronization with the low-mass resonances is not included here, and is discussed in more detail in Sec. VI. The interference between the CP-odd and CP-even contribution integrates out to zero, as reflected in the zero terms in Eq. (31).

Let us conclude this section by discussing the cross section of the $q\bar{q} \to \gamma H$ process as a function of the anomalous couplings summarized in Table VIII. Detecting or setting limits on this process will be of interest for constraining the following couplings, as discussed in Sec. III

³We thank Ian Low for updating the results in Eq. (7) of Ref. [94].

There is a sign change of the $\kappa_2^{Z\gamma}$ coupling when compared to coefficients in common with Ref. [45], because here we use the convention $D_{\mu} = \partial_{\mu} - \mathrm{i} \frac{e}{2s_w} \sigma^i W_{\mu}^i - \mathrm{i} \frac{e}{2c_w} B_{\mu}$, as discussed in Sec. II.

$$\frac{\sigma(q\bar{q} \to \gamma H)}{\sigma_{\text{ref}}^{\gamma H}} = (g_2^{Z\gamma})^2 + (g_4^{Z\gamma})^2 + 0.553(g_2^{\gamma\gamma})^2 + 0.553(g_4^{\gamma\gamma})^2 - 0.578g_2^{Z\gamma}g_2^{\gamma\gamma} - 0.578g_4^{Z\gamma}g_4^{\gamma\gamma}, \tag{32}$$

where the reference cross section is $\sigma_{\rm ref}^{\gamma H}=1.33\times 10^4$ fb. We will investigate this channel further in Sec. VII.

V. LOOP-INDUCED STANDARD MODEL CONTRIBUTIONS

The NLO EW corrections from the PROPHECY4F and HAWK generators have been widely used in calculations of the H boson production and decay cross sections at the LHC and included in the LHC Higgs Working Group recommendations [39]. The corrections are generally positive in the $H \to 4\ell$ process [96] and negative in the VBF and VH processes [97]. Differential distributions also show growth of these effects at higher energy, such as at hightransverse momentum p_T^H of the H boson in the case of VBF and VH production, as expected for the well-known EW Sudakov enhancement. Our goal here is to reexamine some of these effects, focus on certain kinematic distributions, and compare the NLO EW effects to those generated by the EFT operators. In particular, we also produce kinematic distributions with JHUGen at LO, and introduce effective $g_2^{\gamma\gamma,\mathrm{SM}}$ and $g_2^{\mathrm{Z}\gamma,\mathrm{SM}}$ couplings to model what one can call pseudo-EW corrections. Both PROPHECY4F and HAWK include the interference of the loop-induced contributions with the Born process as dictated at NLO accuracy, but do not include squared contributions, which are formally of higher order. Nonetheless, these squared terms may be comparable to or larger than the interference contributions, and we examine this with the effective $g_2^{\gamma\gamma,SM}$ and $g_2^{Z\gamma,SM}$ couplings by keeping or excluding their squared contributions.

The effective pointlike couplings, such as $g_2^{\text{gg,SM}}$, $g_2^{\gamma\gamma,\text{SM}}$, and $q_2^{\text{Zy,SM}}$, can model SM loop effects only in decay (or production) with on-shell particles, such as $H \to gg, \gamma\gamma, Z\gamma$. The numerical values of these couplings from Eq. (1) can be found in Eqs. (15), (19), and (28), respectively. As we illustrate below, these couplings are inadequate for modeling loop effects in decays to virtual vector bosons, such as $H \to \gamma^* \gamma / Z \gamma \to f \bar{f} \gamma$ or $H \to \gamma^* \gamma^* / Z \gamma^* / Z Z \to f \bar{f} f' \overline{f'}$. The nontrivial q^2 dependence of the effective HVV vertex cannot be described this way and the g_2^{ZZ} and other tensor structures appearing in Eq. (1) are not represented. Similar considerations apply to the VBF and VH production, and also to the γH production, as discussed in Sec. III. To make these statements in a quantitative way, we compare a simulation of these effective couplings to a complete modeling of the NLO EW effects.

In order to model the SM loop corrections in the $H \rightarrow$ $f\bar{f}f'\bar{f'}$ process, we employ the PROPHECY4F generator, and in VBF and ZH production we use HAWK. In both cases, the NLO EW corrections can be applied to the process of interest and compared to the LO simulation. We note that HAWK provides all results in the form of binned distributions, since unweighted events are not available and events are not stored in LHE format [98]. This may complicate analysis and comparison of generated events, since different code would have to be employed in calculating the observables. Therefore, we have introduced a software interface which writes weighted events from HAWK simulation in the LHE format, and all further analysis is performed in a unified way. Moreover, photon bremsstrahlung leads to smearing of kinematic distributions. In order to disentangle photon radiation from purely EW effects in kinematic distributions in both the $H \rightarrow 4\ell$ and VH with $V \to \ell^+ \ell^-$ processes, we have introduced a recombination algorithm in analysis of events written in LHE format. The four-momentum of the associated photon is added to the nearest lepton in this algorithm. We note that NLO QCD + EW predictions for ZH production have been recently implemented in the POWHEG framework [99], but are not included in this study.

We start with the study of NLO EW corrections in the $H \rightarrow 2e2\mu$ decay process. In Fig. 6, the LO and NLO EW modeling of the process is shown, as generated with the PROPHECY4F generator, and compared to ad hoc loop correction with $g_2^{\gamma\gamma,\mathrm{SM}}$ and $g_2^{Z\gamma,\mathrm{SM}}$ with JHUGen. The overall correction to the decay width is +1.5%, as shown in Table II. The size of the effect with the pseudo-EW correction of -0.6% is similar, but does not reproduce the sign. However, including the quadratic terms with the pseudo-EW corrections appears important, as there is a growing importance of these effects at $q^2 \rightarrow 0$, which increases the correction by +2.6%. The effect of linear terms appearing with the proper NLO EW corrections is most pronounced in the intermediate m_1 and m_2 ranges, away from the pole of on-shell Z. This is where the effect of interference is most pronounced. Overall, we conclude that the pseudo-EW corrections only roughly model the effect in the $H \rightarrow 2e2\mu$ process of an order of magnitude, but are not adequate to describe the proper EW corrections. Nonetheless, they also indicate that the quadratic terms may become sizable and more important than the linear terms at the values of m_2 of a few GeV or below.

The study of NLO EW corrections in the VBF process is shown in Fig. 7 and in the VH process in Fig. 8, where the LO and NLO EW modeling of the process is shown with the HAWK generator, and compared to $ad\ hoc$ loop correction with $g_2^{\gamma\gamma, \text{SM}}$ and $g_2^{Z\gamma, \text{SM}}$ with JHUGen. The selection requirements are similar to those in Sec. III, except that in VBF we do not place a requirement on q_V^2 and in VH we apply a looser requirement $m_{\ell\ell} > 0.1$ GeV and a tighter

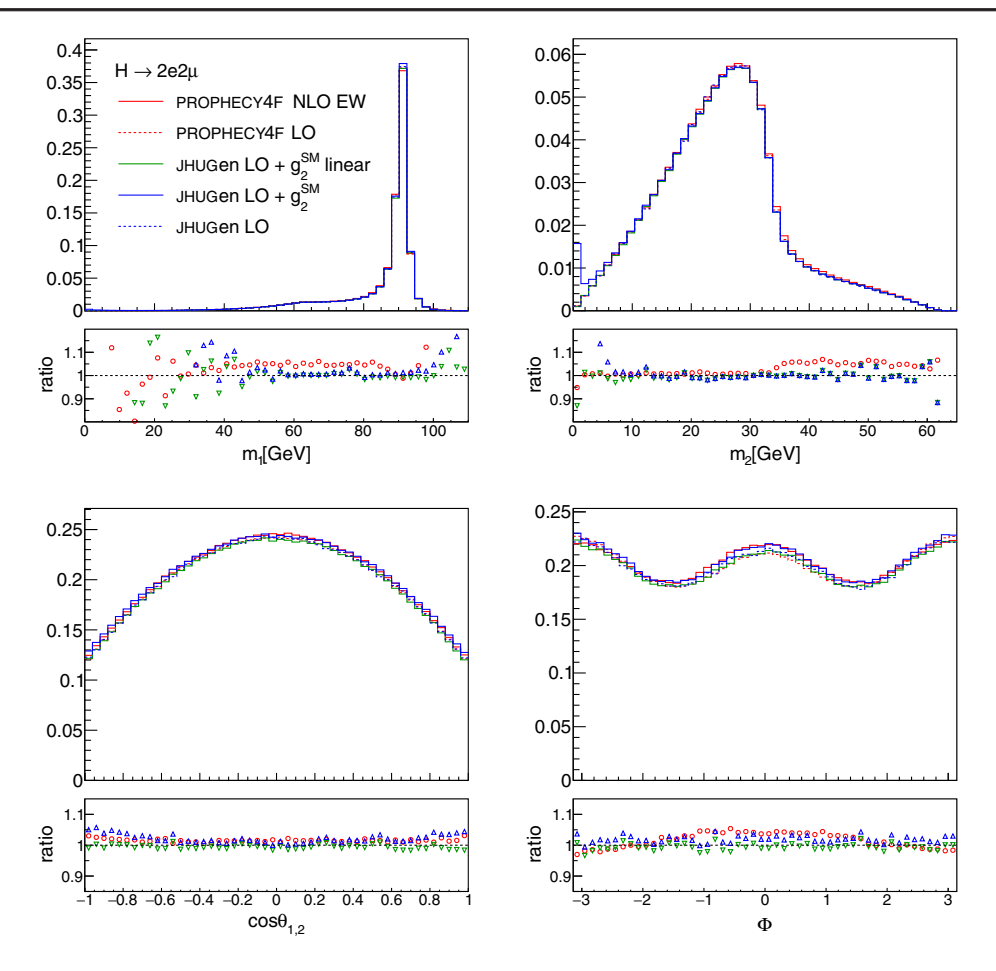


FIG. 6. Distributions of kinematic observables in the $H \to 2e2\mu$ decay: $m_1, m_2, \cos\theta_{1,2}, \Phi$. Five distributions are shown in each case: LO simulation (dashed red), NLO EW (solid red) with PROPHECY4F, LO (dashed blue) and *ad hoc* loop correction with $g_2^{\gamma\gamma, \rm SM}$ and $g_2^{\gamma\gamma, \rm SM}$ with (solid blue) and without (solid green) quadratic terms with JHUGen. Ratio of distributions with and without corrections are also shown.

requirement $p_T^\ell > 5$ GeV. The overall NLO EW correction is negative in the range of 6%–7%, as shown in Table II, and grows in size with energy represented by transverse momentum p_T^H in both cases. In the case of VBF, the momentum of the intermediate vector bosons $\sqrt{-q_{1,2}^2}$ also shows this feature. The pseudo-EW corrections show about -1.2% correction in the VH process and small growth of the effect with p_T^H , but no sizable effect in the VBF process. In both VBF and VH, there is no evidence of importance of the quadratic terms with the $g_2^{\rm SM}$ expansion. We conclude

that the pseudo-EW corrections are not adequate in the VBF and VH processes, even if in the VH process cross section modifications appear in the same direction.

Given the inadequacy of the pseudo-EW corrections, we have investigated an approximate approach of reweighting the LO EW simulation with a dynamic k factor, which is a ratio of the NLO and LO EW kinematic distributions. This approach can capture the main features of the correction, such as its growth with p_T^H , if this quantity is used as the kinematic distribution in reweighting. However, this approach does not guarantee adequate modeling of the

TABLE II. The effect of NLO EW corrections calculated with the PROPHECY4F and HAWK programs in the three processes with the selection requirements discussed in Sec. III. Also shown are the effects of the $g_2^{\gamma\gamma,\text{SM}}$ and $g_2^{Z\gamma,\text{SM}}$ couplings with and without (linear) using their squared contributions calculated with the JHUGen program.

	EW NLO/LO	$(\mathrm{LO} + g_2^\mathrm{SM})/\mathrm{LO}$	$(LO + g_2^{SM} linear)/LO$
$H \to 4\ell$	+1.5%	+2.0%	-0.6%
VBF	-6.7%	+0.2%	+0.1%
$Z(\to \ell^+\ell^-)H$	-6.4%	-1.2%	-1.2%

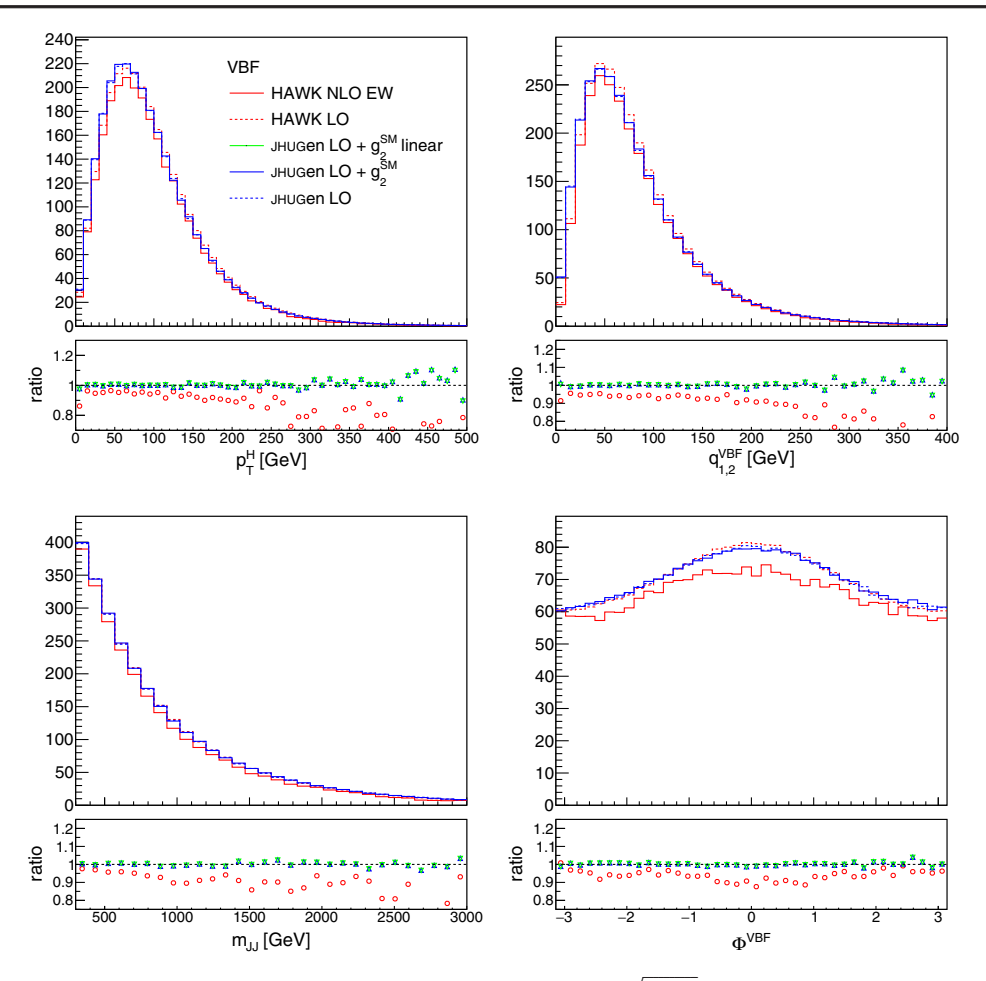


FIG. 7. Distributions of kinematic observables in the VBF production; $p_T(H)$, $\sqrt{-q_{1,2}^2}$, m_{jj} , and Φ^{VBF} . Five distributions are shown in each case: LO simulation (dashed red), NLO EW (solid red) with HAWK, LO (dashed blue) and *ad hoc* loop correction with $g_2^{\gamma\gamma,SM}$ and $g_2^{Z\gamma,SM}$ with (solid blue) and without (solid green) quadratic terms with JHUGen. Ratio of distributions with and without corrections are also shown.

other kinematic distributions simultaneously, if those are not also used in reweighting. For example, we found that reweighting based on p_T^H does not bring angular distributions to an agreement.

The importance of the NLO EW corrections will become evident in the actual analysis of LHC data. The precision of existing LHC constraints [3,46–60] is not sufficient for reaching the NLO EW effects appearing in the SM. Therefore, accurate modeling of such effects may not appear as critical at present. However, with growing precision of experimental measurements a careful investigation of NLO EW effects on kinematic distributions will become important.

VI. CALCULATION OF THE WIDTH IN THE PRESENCE OF INTERMEDIATE PHOTONS

The presence of intermediate photons in H boson decays to fermions via $\gamma^* \to f^+ f^-$ can lead to sharp peaks in the spectrum when $q^2 = (p_{f^+} + p_{f^-})^2$ is small. For decays

into leptons, these peaks are cut off by the physical lepton masses. In the case of quarks, nonperturbative effects wash out this peak structure and introduce hadronic resonances instead. In the following, we introduce a procedure, based on matching amplitudes in the collinear limit, to handle these singularities in a way which allows their efficient numerical evaluation. We draw parts of this description from Ref. [62]. Technical details can be found in Appendix B.

We write the partial H boson decay widths as

$$\Gamma_{H \to 2f2f'} = \frac{1}{2m_H} \frac{1}{(4_{ff'})} \int dPS^{(4)} |\mathcal{M}_{H \to 2f2f'}|^2,$$
 (33)

$$\Gamma_{H\to 2f\gamma} = \frac{1}{2m_H} \int dPS^{(3)} |\mathcal{M}_{H\to 2f\gamma}|^2, \qquad (34)$$

$$\Gamma_{H \to \gamma \gamma} = \frac{1}{2m_H} \frac{1}{(2_{\gamma \gamma})} \int dP S^{(2)} |\mathcal{M}_{H \to \gamma \gamma}|^2, \quad (35)$$

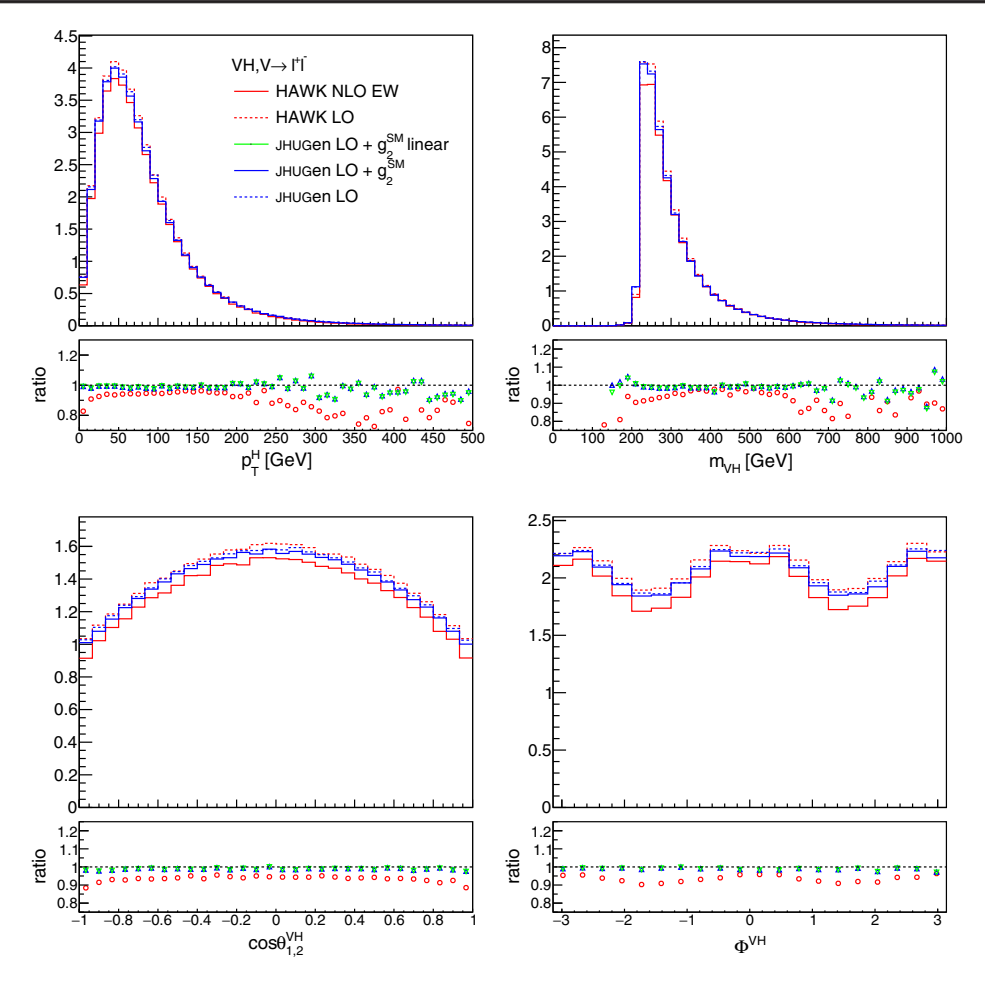


FIG. 8. Distributions of kinematic observables in VH production: $p_T(H)$, m_{VH} , $\cos\theta_{1,2}^{VH}$, and Φ^{VH} . Five distributions are shown in each case: LO simulation (dashed red), NLO EW (solid red) with HAWK, LO (dashed blue) and *ad hoc* loop correction with $g_2^{\gamma\gamma, \rm SM}$ and $g_2^{\rm Z\gamma, SM}$ with (solid blue) and without (solid green) quadratic terms with JHUGen. Ratio of distributions with and without corrections are also shown.

where we introduced the symbols $(j_{pp'}) = j^{\delta_{pp'}}$ for symmetry factors for identical particles. Explicit parametrization of the phase spaces, using appropriate variables, yields

$$\int dPS^{(3)} = \int_{4m_1^2}^{M_H^2} \frac{dq_{12}^2}{2\pi} \int dPS^{(2)}(M_H^2, q_{12}^2, 0)$$

$$\times dPS^{(2)}(q_{12}^2, m_f^2, m_f^2), \qquad (36)$$

and

$$\int dPS^{(4)} = \int_{4m_f^2}^{M_H^2} \frac{dq_{12}^2}{2\pi} \int_{4m_{f'}^2}^{(M_H^2 - \sqrt{q_{12}})^2} \frac{dq_{34}^2}{2\pi}$$

$$\times \int dPS^{(2)}(M_H^2, q_{12}^2, q_{34}^2)$$

$$\times dPS^{(2)}(q_{12}^2, m_f^2, m_f^2) dPS^{(2)}(q_{34}^2, m_{f'}^2, m_{f'}^2),$$
(37)

where $dPS^{(2)}(q^2, m_1^2, m_2^2) = d\cos\theta d\phi/(2q^2)$. We split the invariant mass integrations in Eqs. (36) and (37) into a lowand high-virtuality region

$$\int_{4m^2}^{M^2} dq_{\gamma}^2 = \int_{4m^2}^{\mu^2} dq_{\gamma}^2 + \int_{\mu^2}^{M^2} dq_{\gamma}^2$$
 (38)

separated by an arbitrary parameter $\mu^2 \ll M^2$. In this form, we can apply the collinear approximation to the squared

matrix elements $|\mathcal{M}_{X+\gamma^*\to X+2f}|^2 \stackrel{q_{\gamma^*}^2\ll \mu^2}{\longrightarrow} P_{ff}(z)/q_{\gamma^*}^2 \times |\mathcal{M}_{X+\gamma}|^2$ in the low-virtuality region and analytically integrate over q_{γ}^2 [62]. The high-virtuality region does not contain sharp peaks and can be treated numerically in a standard manner. As a result, the partial decay width for $H\to 2\ell\gamma$ can be written as

$$\Gamma_{H\to 2\ell\gamma} = \Gamma_{H\to 2\ell\gamma} \bigg|_{q_{2\ell}^2 \ge \mu^2} + \frac{\alpha}{2\pi} \left[\frac{2}{3} \log \left(\frac{\mu^2}{m_{\ell}^2} \right) - \frac{10}{9} \right] 2\Gamma_{H\to \gamma\gamma} + \mathcal{O}(\mu^2/M_H^2), \tag{39}$$

where the left-hand side is independent of μ^2 . We note that the low virtuality region is conveniently expressed in terms of an analytic function containing a potentially large $\log(m_{\mathscr{C}}^2)$ times the width $\Gamma_{H\to\gamma\gamma}$, which can be straightforwardly obtained using numerical methods for any

combination of anomalous couplings [Eq. (17)]. Contributions from low virtuality Z bosons decaying into 2ℓ are parametrically suppressed by μ^2/M_H^2 . In a similar fashion, we obtain the results for the H boson decays into four leptons

$$\Gamma_{H \to 2\ell'2\ell'} = \Gamma_{H \to 2\ell'2\ell'} \Big|_{q_{2\ell'}^2 \ge \mu^2, q_{2\ell'}^2 \ge \mu^2} + \frac{\alpha}{2\pi} \left[\frac{2}{3} \log \left(\frac{\mu_{\ell'}^2}{m_{\ell'}^2} \right) - \frac{10}{9} \right] \Gamma_{H \to 2\ell'\gamma} \Big|_{q_{2\ell'}^2 \ge \mu^2} + \frac{\alpha}{2\pi} \left[\frac{2}{3} \log \left(\frac{\mu_{\ell''}^2}{m_{\ell''}^2} \right) - \frac{10}{9} \right] \Gamma_{H \to 2\ell'\gamma} \Big|_{q_{2\ell'}^2 \ge \mu^2} + \left(\frac{\alpha}{2\pi} \right)^2 \left[\frac{2}{3} \log \left(\frac{\mu_{\ell'}^2}{m_{\ell'}^2} \right) - \frac{10}{9} \right] \left[\frac{2}{3} \log \left(\frac{\mu_{\ell''}^2}{m_{\ell''}^2} \right) - \frac{10}{9} \right] 2\Gamma_{H \to \gamma\gamma} + \mathcal{O}(\mu^2/M_H^2), \tag{40}$$

$$\begin{split} \Gamma_{H \to 4\ell} &= \Gamma_{H \to 4\ell} \bigg|_{q_{2\ell}^2 \ge \mu^2} + \frac{\alpha}{2\pi} \left[\frac{2}{3} \log \left(\frac{\mu^2}{m_{\ell}^2} \right) - \frac{10}{9} \right] \Gamma_{H \to 2\ell\gamma} \bigg|_{q_{2\ell}^2 \ge \mu^2} \\ &+ \left(\frac{\alpha}{2\pi} \right)^2 \left[\frac{2}{3} \log \left(\frac{\mu^2}{m_{\ell}^2} \right) - \frac{10}{9} \right]^2 \Gamma_{H \to \gamma\gamma} + \mathcal{O}(\mu^2 / M_H^2). \end{split} \tag{41}$$

If the H boson decay occurs into quark final states, the low virtuality region is affected by sizable nonperturbative effects, which can be related to the experimentally measured quantity $\Delta\alpha_{\rm had}^{(5)}(M_Z^2)$ via a dispersion relation and unitarity [62]. The value of $\Delta\alpha_{\rm had}^{(5)}(M_Z^2)=(276.11\pm1.11)\times10^{-4}$ [100,101] has been extracted from the lowenergy region of the ratio $\sigma(e^+e^-\to {\rm hadrons})/\sigma(e^+e^-\to \mu^+\mu^-)$ and is related to the fine structure constant via $\alpha(s)=\alpha(0)/(1-\Delta\alpha(s))$. Summing over the five light quark flavors, labeling $\sum_q \Gamma_{H\to 2q\gamma}=\Gamma_{H\to 2j\gamma}$, and choosing $\mu^2\gg 4m_b^2$, we find

$$\Gamma_{H\to 2j\gamma} = \Gamma_{H\to 2j\gamma} \bigg|_{q_{2q}^2 \ge \mu^2} + \left[\Delta \alpha_{\text{had}}^{(5)}(M_Z^2) + \frac{\alpha}{\pi} \frac{11}{9} \log \left(\frac{\mu^2}{M_Z^2} \right) \right] \times 2\Gamma_{H\to \gamma\gamma} + \mathcal{O}(\mu^2/M_Z^2), \tag{42}$$

and similar for $\Gamma_{H\to 4j}$.

In order to illustrate the performance of Eq. (39), we model the $H \to 2\ell\gamma$ decay with the HVV couplings corresponding to $g_2^{\gamma\gamma, {\rm SM}}$ and $g_2^{Z\gamma, {\rm SM}}$ as defined in Eqs. (19) and (28). We scan the value of cutoff μ^2 in Eq. (39) from the threshold value of $(2m_\ell)^2$ up to $(5~{\rm GeV})^2$ for both electrons ($\ell=e$) and muons ($\ell=\mu$). Figure 9 shows the first two terms appearing in Eq. (39), the value of $\Gamma_{H\to 2\ell\gamma}$ with the requirement $q_{2\ell}^2 \ge \mu^2$ and the value of $\Gamma_{H\to \gamma\gamma}$ multiplied by the μ^2 -dependent factor. The other terms in Eq. (39) can be neglected in this comparison. With the μ^2 increasing, the former cross section falls while the latter rises, leading to a constant cross section of the $H\to 2\ell\gamma$ process, as one would expect to observe for the proper modeling of the effect.

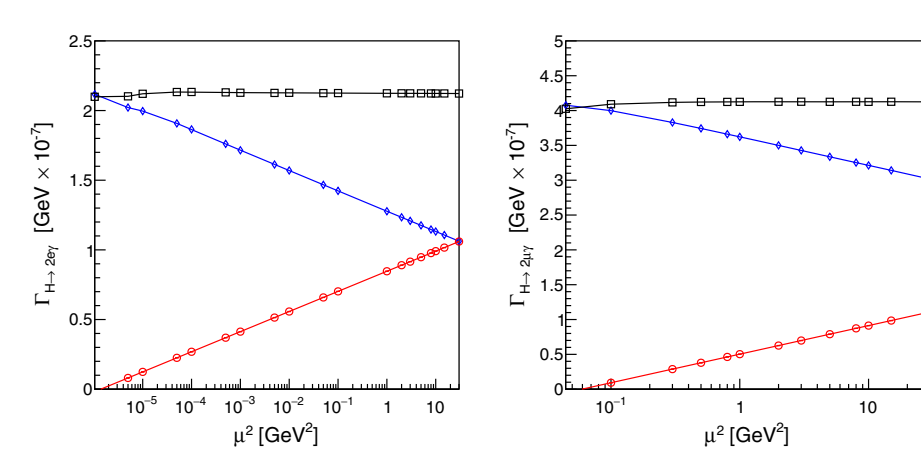


FIG. 9. The partial decay width of the process $H \to 2\ell\gamma$ calculated using Eq. (39) for the $2e\gamma$ (left) and $2\mu\gamma$ (right) final states with the couplings discussed in text. The first two terms appearing in Eq. (39) are shown for several values of μ^2 : $\Gamma_{H\to 2\ell\gamma}$ with the requirement $q_{2\ell}^2 \ge \mu^2$ (blue diamonds) and $\Gamma_{H\to\gamma\gamma}$ multiplied by the μ^2 -dependent factor (red circles). The sum of the cross sections is also shown (black squares).

In order to illustrate the performance of Eqs. (40) and (41), we model the $H \to 2e2\mu$, 4e, and 4μ decays with the $g_4^{\gamma\gamma}$ and $g_4^{Z\gamma}$ couplings set to the values of $g_2^{\gamma\gamma, \rm SM}$ and $g_2^{Z\gamma, \rm SM}$, respectively, as used in the previous test. Both in this test and in the previous test of Eq. (39), the rationale is to model the processes involving virtual photons which exhibit growth with $q^2 \to 0$. We choose to illustrate the performance with CP-even couplings in one case and CP-odd couplings in the other, but the procedure has been validated to work in any combination of couplings. The $\kappa_2^{Z\gamma}$ coupling formally involves a virtual photon. However, due to appearance of q_γ^2 in the numerator of the tensor structure in Eq. (1), this coupling does not exhibit divergence with $q^2 \to 0$. Its behavior is similar to the terms with the virtual Z and can be absorbed in the corresponding terms.

As before, we scan the value of cutoff μ^2 in Eq. (40) for the $H \rightarrow 2e2\mu$ process and in Eq. (41) for the $H \rightarrow 4e$ and 4μ processes from the threshold value of $(2m_{\ell})^2$ up to (5 GeV)². The threshold value is defined for muons in the case of $H \rightarrow 4\mu$ and electrons in the other two cases. Figure 10 shows the partial decay width of the process $H \rightarrow 2e2\mu$ calculated using Eq. (40), and $H \rightarrow 4e$ and 4μ calculated using Eq. (41). Several terms in the corresponding equations are isolated: the first term in each equation is shown with the requirement $q_{2\ell}^2 \ge \mu^2$ common for electrons and muons; the $\Gamma_{H \to \gamma \gamma}$ multiplied by the μ^2 -dependent factor, the $\Gamma_{H\to 2e\gamma}$ with the requirement $q_{2e}^2 \geq \mu^2,$ and the $\Gamma_{H\to 2\mu\gamma}$ with the requirement $q_{2\mu}^2 \ge \mu^2$, where both $\Gamma_{H\to 2\ell\gamma}$ are multiplied by the μ^2 -dependent factor as well. With the μ^2 increasing, the first term falls while the other terms generally rise. Again, we obtain a constant cross section of the four-lepton process, as one would expect to observe for the proper modeling of the effect.

The combination of formulas in Eqs. (39) and (42) for $\Gamma_{H\to 2f\gamma}$, and Eqs. (40), (41), and similar ones involving hadronic jets for $\Gamma_{H\to 4f}$ should allow one to handle low- q^2 singularities and hadronic structure with efficient numerical evaluation.

VII. EXPECTED CONSTRAINTS ON THE COUPLINGS WITH PHOTONS

We continue by investigating the on-shell production and decay of the H boson with its couplings to weak vector bosons in the VBF, VH, and $H \rightarrow VV \rightarrow 4\ell$ processes. There has already been extensive study of the HVV couplings, both by experimental collaborations and in phenomenological work. However, there was no conclusive study on the effects of the photon contribution in the production topology. In our previous work in Ref. [45], we pointed out that the decays $H \rightarrow \gamma \gamma$ and $Z\gamma$ with on-shell photons provide constraints on the $g_2^{\gamma\gamma}$, $g_4^{\gamma\gamma}$, $g_2^{Z\gamma}$, and $g_4^{Z\gamma}$ couplings which are stronger than those that can be obtained from the VBF, VH, and $H \rightarrow 4\ell$ processes. For this reason, the analysis of multiple operators was simplified by setting those four couplings to zero. The constraints from the decays with on-shell photons can be illustrated with the simplified partial decay width expressions in Eqs. (23) and (30). This effect in the $H \to 4\ell$ was studied with LHC data [48] and with phenomenological tools [25,35]. In the following we reexamine the $H \to 4\ell$ decay and investigate the VBF and VH processes.

First, we would like to point to the effect already observed in Tables IV, V, and VI. Let us focus on any of the three operators C_{HW} , C_{HWB} , or C_{HB} where the g_2^{ZZ} , $g_2^{Z\gamma}$, and $g_2^{\gamma\gamma}$ couplings contribute, or equivalently any of $C_{H\tilde{W}}$, $C_{H\tilde{W}B}$, or $C_{H\tilde{B}}$, where g_4^{ZZ} , $g_4^{Z\gamma}$, and $g_4^{\gamma\gamma}$ contribute.

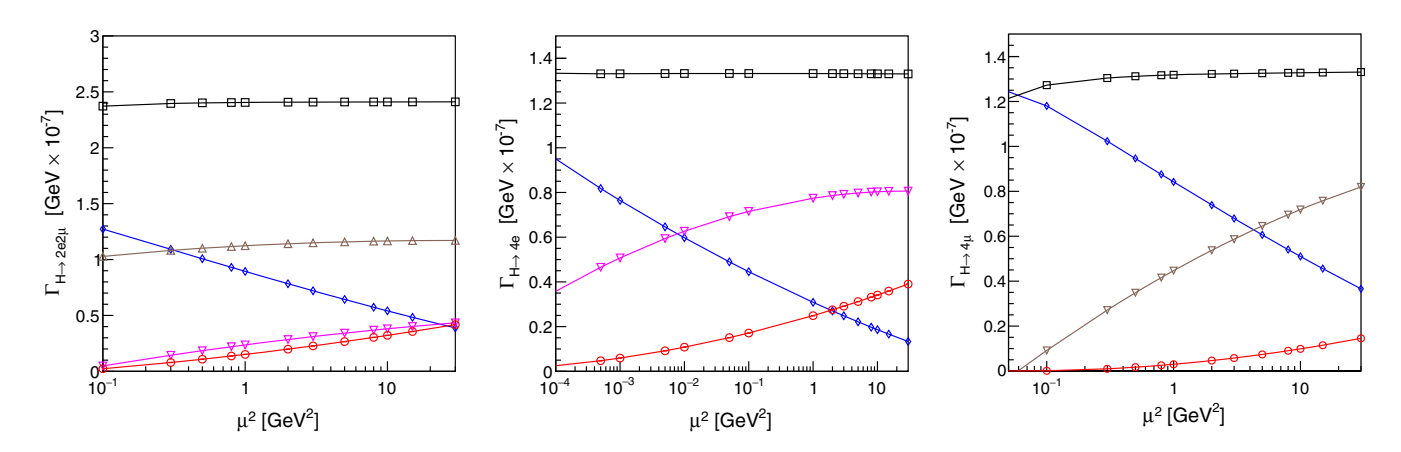


FIG. 10. The partial decay width of the process $H \to 2e2\mu$ calculated using Eq. (40) (left), $H \to 4e$ (middle) and $H \to 4\mu$ (right) calculated using Eq. (41) with the couplings discussed in text. The first term in each equation is shown with the requirement $q_{2\ell}^2 \ge \mu^2$ common for electrons and muons (blue diamonds). The following terms multiplied by the μ^2 -dependent factors are also shown: the $\Gamma_{H\to\gamma\gamma}$ (red circles), the $\Gamma_{H\to2e\gamma}$ with the requirement $q_{2e}^2 \ge \mu^2$ (magenta triangles pointing down), and the $\Gamma_{H\to2\mu\gamma}$ with the requirement $q_{2\mu}^2 \ge \mu^2$ (brown triangles pointing up). The sum of the cross sections is also shown (black squares).

While the $g_{2,4}^{ZZ}$ contributions to the VBF and VH processes are comparable and sometimes even dominant for a given C_{HX} operator, their contributions to the $H \to 4\ell$ decay appear to be negligible in comparison. For photon couplings, the reverse is the case, their contribution to decay is much larger than to production. Therefore, the photon couplings have relatively higher importance in decay compared to the production processes. This still does not tell us if the photon couplings are better constrained in production or decay, and this is what we investigate below.

In the following, prospects with either 3000 fb⁻¹ (HL-LHC) or 300 fb⁻¹ (full LHC) are studied at a 13 TeV collision energy. We use the JHUGen simulation to model the VBF, WH, ZH/γ^*H , γH , and gluon fusion production with the decay $H \to 4\ell$. We include the effective background with the POWHEG [102] simulation of the $q\bar{q} \to 4\ell$ process, which we scale to match the contributions of other processes as found in experiment, such as $gg \to 4\ell$ and Drell-Yan Z production [103]. The detector effects are modeled with $ad\ hoc$ acceptance selection and empirical efficiency corrections, and the lepton and hadronic jet momenta are smeared to achieve realistic resolution effects. The following selection requirements are applied: $p_T^e > 5$ GeV, $p_T^\mu > 7$ GeV, $p_T^{\rm jet} > 30$ GeV, $|\eta^e| < 2.5$, $|\eta^\mu| < 2.4$, $|\eta^{\rm jet}| < 4.7$, $|m_{\ell\ell}| > 12$ GeV, $|m_{4\ell} - m_H| < 3.5$ GeV.

We target the optimal analysis of four anomalous couplings expressed through the fractional contributions to the $H \to 2e2\mu$ process $f_{g2}^{Z\gamma}$, $f_{g2}^{\gamma\gamma}$, $f_{g4}^{Z\gamma}$, and $f_{g4}^{\gamma\gamma}$, with the approach similar to Ref. [45]. The cross section fractions are defined following

$$f_{gn} = \frac{g_n^2 \alpha_{nn}^{(f)}}{\sum_i g_i^2 \alpha_{ii}^{(f)}} \operatorname{sign}\left(\frac{g_n}{g_1}\right),\tag{43}$$

where the $\alpha_{nn}^{(f)}$ coefficients are introduced in Eq. (11) for the final state (f). The numerical values of these coefficients are given in Table III, where they are normalized with respect to the α_{11} coefficient, corresponding to the cross section calculated for $g_1 = 1$. The α_{nn} are the cross sections for $g_n = 1$. In Table III, we also quote the cross section ratios defined in VBF and VH production for comparison. As noted above and evident from this table, the relative importance of photon couplings is higher in decay compared to production.

For simplicity, we set the contributions of the other anomalous contributions to zero: $f_{g2}^{ZZ} = f_{g4}^{ZZ} = f_{\Lambda 1}^{ZZ} = f_{\Lambda 1}^{ZZ} = 0$. This assumption will provide tighter constraints than one could achieve otherwise, but this is sufficient for comparison to the precision obtained from $H \to \gamma \gamma$ and $Z\gamma$ following Eqs. (23) and (30). We use the relationship with $\Delta M_W = 0$ in Eq. (5) for the SM-like contribution, but we do not enforce the $SU(2) \times U(1)$ symmetry in Eqs. (6)–(9)

TABLE III. List of anomalous $HZ\gamma$ and $H\gamma\gamma$ couplings g_n , cross section fractions f_{gn} , and the cross section ratio α_{nn}/α_{11} defined in $H\to 2e2\mu$ decay, VBF, and $q\bar{q}\to ZH/\gamma^*H$ production. For comparison, the $g_4^{\rm ZZ}$ coupling is also shown. The requirements $m_{\ell\ell}>4$ GeV and $p_T^{\rm jet}>1$ GeV are introduced in $\alpha_{nn}^{(f)}$ and $\alpha_{nn}^{(i)}$ calculation by convention.

Coupling g_n	Fraction f_{gn}	$\begin{array}{c} H \to 2e2\mu \\ \alpha_{nn}^{(f)}/\alpha_{11} \end{array}$	${ m VBF} lpha_{nn}^{(i)}/lpha_{11}$	$ZH/\gamma^*H \ lpha_{nn}^{(i)}/lpha_{11}$
$g_2^{\gamma\gamma}$	$f_{g2}^{\gamma\gamma}$	355.1	65.04	2.330
$g_2^{Z\gamma}$	$f_{g2}^{Z\gamma}$	438.5	24.89	50.51
$g_4^{\gamma\gamma}$	$f_{g4}^{\gamma\gamma}$	348.0	64.28	1.790
$g_4^{Z\gamma}$	$f_{g4}^{Z\gamma}$	356.7	23.44	32.50
g_4^{ZZ}	f_{g4}^{ZZ}	0.153	11.27	47.94

and instead set $g_2^{WW}=g_4^{WW}=\kappa_1^{WW}=\kappa_2^{Z\gamma}=0$. This is done to isolate the contributions with genuine photon couplings, which exhibit the features of virtual photons. These are the contributions which also appear and are constrained in the $H\to Z\gamma$ and $\gamma\gamma$ processes.

A. Expected constraints on photon couplings from $H \rightarrow VV \rightarrow 4\ell'$ decay

We build the analysis following the MELA approach with the two types of optimal discriminants, using the full kinematic information in the four-lepton decay. There are four discriminants $\mathcal{D}_{g2}^{Z\gamma}$, $\mathcal{D}_{g2}^{\gamma\gamma}$, $\mathcal{D}_{g4}^{Z\gamma}$, and $\mathcal{D}_{g4}^{\gamma\gamma}$ which are designed to separate the pure anomalous contributions from the SM-like, and there are four interference discriminants $\mathcal{D}_{\text{int}}^{Z\gamma}$, $\mathcal{D}_{\text{int}}^{\gamma\gamma}$, $\mathcal{D}_{CP}^{Z\gamma}$, $\mathcal{D}_{CP}^{\gamma\gamma}$ which isolate interference of the SM with the same four anomalous contributions. The full available information is used in calculating the discriminants, and further details on the MELA approach can be found in Ref. [45] and references therein. In this and further analyses discussed below, events are split into the $H \rightarrow 2e2\mu$, 4e, and 4 μ categories, which is an important aspect because the relative fractions of events between these types change with anomalous couplings, due to interference of diagrams with identical leptons in the 4e and 4μ final states. In the end, for each event in a category j, a set of observables x is defined.

Since analysis of decay information is essentially independent from the production mechanism, we model kinematic distributions using simulation of the gluon fusion process. However, in Sec. VII B we will also show how the full production and decay information can be taken into account. The probability density function for the signal decay process in gluon fusion production, before proper normalization, is defined as

ggH:
$$\mathcal{P}(\mathbf{x}; \vec{f}) \propto \sum_{k,l=1 \atop k \neq l}^{K} \mathcal{P}_{kl}(\mathbf{x}) \sqrt{|f_{gk} \cdot f_{gl}|} \operatorname{sign}(f_{gk} \cdot f_{gl}),$$
 (44)

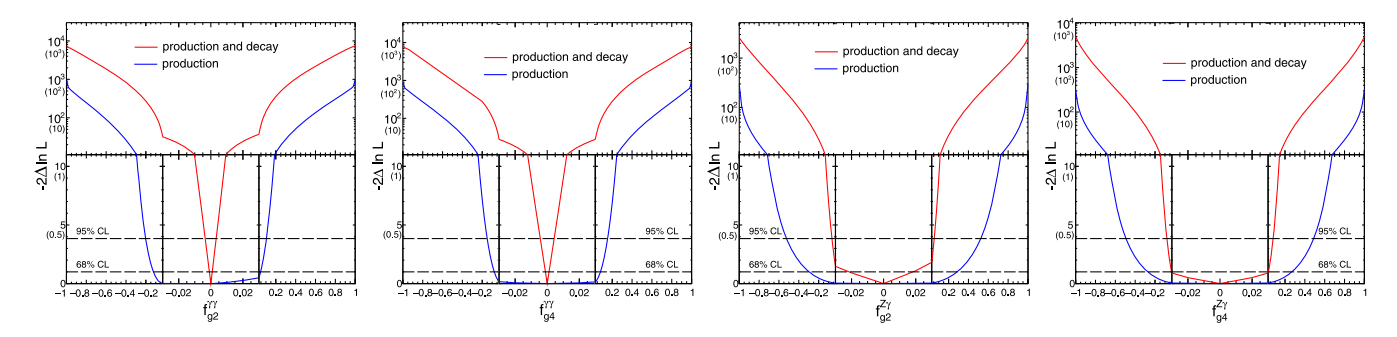


FIG. 11. Expected constraints from a simultaneous fit of $f_{g2}^{\gamma\gamma}$, $f_{g2}^{\gamma\gamma}$, $f_{g2}^{\gamma\gamma}$, and $f_{g4}^{\gamma\gamma}$ using associated production and $H \to 4\ell$ decay with 3000 (300) fb⁻¹ data at 13 TeV. Two scenarios are shown: using MELA observables with production and decay (red) or production only (blue) information. The dashed horizontal lines show the 68 and 95% confidence level (CL) regions.

where \mathbf{x} are the observables and f_{gn} are the cross section fractions of the couplings, K = 5 for the four anomalous couplings and one SM coupling. Equation (44) is obtained from Eq. (11), where the width and Hgg couplings are absorbed into the overall normalization. In gluon fusion production, the electroweak HVV couplings appear only in decay. Therefore, there are 15 terms in Eq. (44). To populate the probability distributions, we use a simulation of unweighted events of several samples that adequately cover the phase space and reweight those samples using the MELA package to parametrize the other terms. As in Ref. [45], we implement a cutting planes algorithm [104] using the Hom4PS [105–107] and Gurobi [108] programs to ensure that the probability density function remains positive definite for all possible values of f_{qn} . With 3000 fb⁻¹ data at 13 TeV, we expect about 4500 events reconstructed in the $H \to 4\ell$ channel. In Fig. 11 we show the expected constraints on the four parameters of interest expressed through effective factions $f_{g2}^{\gamma\gamma},\,f_{g4}^{\gamma\gamma},\,f_{g2}^{Z\gamma},$ and $f_{g4}^{Z\gamma}.$ However, before discussing the results, we should turn to analysis of production information.

B. Expected constraints on photon couplings from VBF and VH production

While analysis of the $H \rightarrow 4\ell$ decay can be performed inclusively, the VBF and VH production channels require

analysis of associated particles. Therefore, we follow the approach adopted in our earlier studies [45] to categorize events using the jet information to create the two-jet categories of events enhanced in either VBF or VH events with hadronic decay of the V, respectively. In addition, the leptonic VH, one-jet VBF, and boosted categories are defined, where $p_T^{4\ell} > 120$ GeV is used to select the latter [45]. The remaining events constitute the untagged category.

We build the analysis following the MELA approach with the two types of optimal discriminants, as discussed for decay above, using the full kinematic information in both the production and the four-lepton decay. In the VBF and VH topologies with two associated jets, both production and decay information are used, except for the interference discriminants, where production information is chosen. In the untagged category, the $H \rightarrow 4\ell$ information is used as in Sec. VII A, and in the other categories the transverse momentum $p_{T}^{4\ell}$ is used.

In the case of the VBF and VH processes, the HVV coupling appears on both the production and decay sides. Therefore, the amplitude squared has a product of four couplings. Equation (45) is obtained from Eq. (11) and has 70 terms,

VBF, VH:
$$\mathcal{P}(\mathbf{x}; \vec{f}) \propto \sum_{\substack{k,l,m,n=1\\k \leq l \leq m \leq n}}^{K} \mathcal{P}_{klmn}(\mathbf{x}) \sqrt{|f_{gk} \cdot f_{gl} \cdot f_{gm} \cdot f_{gn}|} \operatorname{sign}(f_{gk} \cdot f_{gl} \cdot f_{gm} \cdot f_{gn}),$$
 (45)

where the notation follows Eq. (44).

In addition to the joint analysis of production and decay, we also perform an analysis with production information only. In order to achieve this, no decay information is used in the construction of discriminants, and only the total yield of events is used in the untagged category. It is not possible to completely decouple the analysis from decay

information, as for example the relative fraction of $2e2\mu$ events is sensitive to couplings in the decay amplitude. For example, there is a strong destructive interference between the two diagrams with permutation of identical leptons in the $H \rightarrow 4e/4\mu$ decay with the $H\gamma\gamma$ couplings, as illustrated in Fig. 2 and Sec. III, which leads to a modification of the $2e2\mu$ yield faction. However, such dependence on

anomalous couplings is greatly reduced with consideration of yields only.

In Fig. 11 we show the expected constraints on the four parameters of interest $f_{g2}^{\gamma\gamma}$, $f_{g4}^{\gamma\gamma}$, $f_{g2}^{Z\gamma}$, and $f_{g4}^{Z\gamma}$ with 300 and 3000 fb⁻¹ data at 13 TeV, where for comparison constraints from production information alone are shown separately from the full constraints using both decay and production. The information contained in decay can be deduced from the difference of the two constraints, with one exception. The analysis of production information is sensitive to the relative fraction of the $H \rightarrow 2e2\mu$, 4e, and 4μ events. We observe that in the case of the $H \rightarrow \gamma^*\gamma^* \rightarrow 4e$ and 4μ processes, there is a sizable effect of interference between diagrams with permutations of the leptons. This effect in decay competes with information from production in constraining $g_2^{\gamma\gamma}$ and $g_4^{\gamma\gamma}$. We do not find such an effect to be important in constraining $g_2^{Z\gamma}$ and $g_4^{Z\gamma}$ and $g_4^{Z\gamma}$

What we observe is that the constraints from decay are significantly more powerful than from production when both are analyzed with the same channel $H \to 4\ell$. This happens for two reasons. First of all, all reconstructed events contain decay information, while only a small fraction carry production information. Second, the ratio $\alpha_{nn}^{(i)}/\alpha_{11}$ is reduced compared to the same ratio in decay to the trend observed for the ZZ couplings (see, for example, Fig. 10 of Ref. [45]), as indicated with the g_4^{ZZ} example in Table III. This trend explains the tighter constraints on the anomalous ZZ couplings using production information, as opposed to decay. For the same reason, the constraints on the photon couplings $(H\gamma\gamma)$ and $HZ\gamma$ are tighter in decay compared to production.

In Fig. 12, these results for the joint analysis of production and decay are interpreted in terms of constraints on the g_i couplings. As indicated above, these constraints are dominated by decay information, and the results would look similar if only decay information were employed. This

interpretation uses the full expression in Eq. (11), including the total H boson width dependence on anomalous couplings appearing in the denominator, using expressions obtained in Sec. IV. It is assumed that there no decays of the H boson to unknown particles.

We should point out that while decay information is limited to $H \rightarrow VV$ channels only, production information can be obtained by combining all possible decay channels of the H boson, such as $H \to 4\ell$, $\gamma\gamma$, $b\bar{b}$, $\tau^+\tau^-$, and W^+W^- . In this study, we investigate only the $H \to 4\ell$ channel, but the relative importance of production information will increase as other channels are analyzed. This observation is also valid for analysis of the γH production, discussed next. At the same time, the $H \to 4\ell$ channel can also be further optimized for the measurements of the photon couplings by relaxing the invariant mass and transverse momentum constraints on the leptons. For example, the requirement $|m_{\ell\ell}| > 12$ GeV can be relaxed to $|m_{\ell\ell}| >$ 4 GeV, or even further, with significant gain in sensitivity to the $H\gamma\gamma$ and $HZ\gamma$ couplings, as can be seen from the invariant mass m_1 and m_2 distributions in Fig. 2.

C. Expected constraints on photon couplings from γH production

Setting constraints on or measuring the rate of the γH production is interesting on its own, as this production mechanism of the H boson has not been tested on the LHC, in part because its SM rate is not accessible yet. In addition, we would like to assess the feasibility of the $g_2^{\gamma\gamma}$, $g_4^{\gamma\gamma}$, $g_2^{Z\gamma}$, and $g_4^{Z\gamma}$ coupling measurement in this production process. In order to simplify these estimates and because NLO EW event simulation is not available for the γH process yet, we assume that the SM contributions are small compared to the accessible values and thus can be absorbed into these effective pointlike couplings. The validity of these assumptions can be checked against the expected constraints. Single loop calculations of the SM production cross section of $q\bar{q} \rightarrow \gamma H$ predict a cross section of less than 5 fb at the

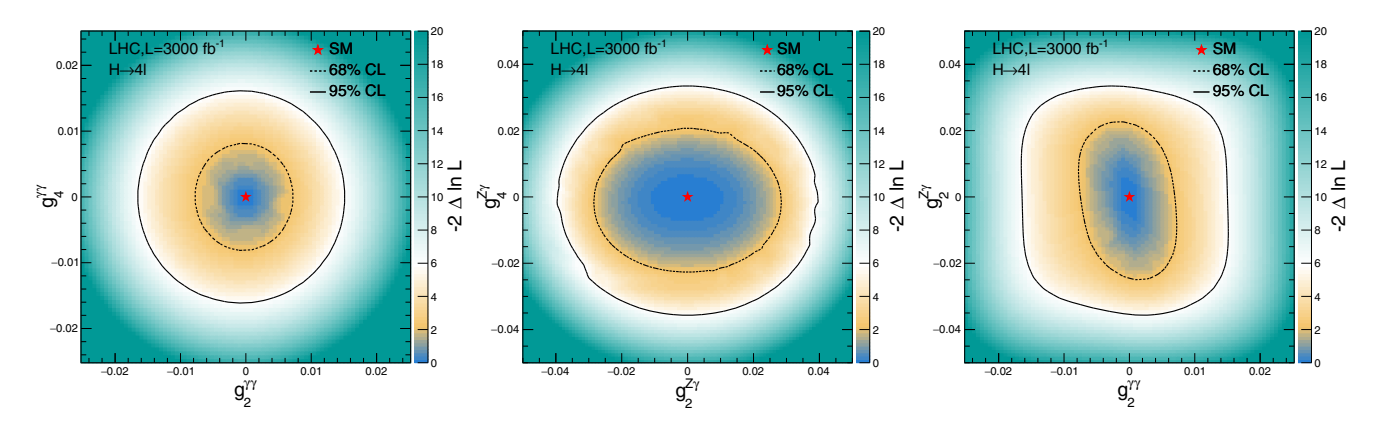


FIG. 12. Expected two-dimensional constraints from a simultaneous fit of $g_2^{\gamma\gamma}$, $g_4^{\gamma\gamma}$, $g_2^{Z\gamma}$, and $g_4^{Z\gamma}$ using decay and production information as shown in Fig. 11.

LHC [109], which corresponds to less than two $H \to 4\ell$ event at the HL-LHC before any selection requirements are applied.

Experimentally, the main distinguishing feature of the γH production mechanism is a high-momentum isolated photon, and we found that the requirement $p_T^{\gamma} > 400$ GeV keeps about 12% of signal events, which corresponds to about 0.9 signal events for $g_2^{\gamma\gamma} = 0.1$ and 0.11 background events with $H \to 4\ell$ and 3000 fb⁻¹ data at 13 TeV. Therefore, for feasibility studies, we identify an additional category of events with a good isolated photon candidate associated with the H boson candidate and the above p_T^{γ} requirement.

Since kinematic features of events do not differ between CP-odd and CP-even couplings and the difference between the $HZ\gamma$ and $H\gamma\gamma$ couplings is weak, we perform a simple fit for excess of events over background without using kinematic distributions. The expected number of signal events is expressed through couplings as the product of coupling modifies on the decay and production sides. These expressions are similar to those in Eqs. (31) and (32), but differ in two aspects. Equation (31) has to be adjusted for the $H \rightarrow 4\ell$ final state instead of the inclusive four-fermion final state and include the effect of acceptance requirements on the lepton quantities, as listed above. Equation (32) has to take into account the effects of the photon acceptance efficiency.

With the above assumptions, the expected two-dimensional constraints on $(g_2^{\gamma\gamma},g_4^{\gamma\gamma})$, $(g_2^{Z\gamma},g_4^{Z\gamma})$, and $(g_2^{Z\gamma},g_2^{\gamma\gamma})$ are shown in Fig. 13. The expected γH constraints with the $H\to 4\ell$ channel alone are not as powerful as those obtained from decay and shown in Fig. 12. However, while this difference is sizable in the case of the $H\gamma\gamma$ couplings, the difference is not as large in the case of the $HZ\gamma$ couplings. Moreover, these constraints are comparable and even better than those obtained from production information in the VBF and VH channels. In both cases, significant gain will result from the analysis of the other H boson decay channels, which are not

considered in this feasibility study. Therefore, it is important to proceed with analysis of VBF, VH, and γH production in all accessible H boson final states.

Searches for heavy resonances decaying into a photon and a hadronically decaying *H* boson have been performed on the LHC [110,111], where the topology of the final state overlaps with the process of our interest, but the interpretation of the results is very different. A reinterpretation of these resonance-search results in terms of the EFT couplings of the *H* boson was attempted in Ref. [84]. However, this study makes crude approximations in its interpretation of LHC data, uses a different set of parameters in a different basis, applies additional symmetry considerations, and is limited to *CP*-even couplings only, making a direct comparison with our results difficult.

D. Expected constraints on photon couplings from decays with on-shell photons

The above results can be compared to possible constraints from the measurements of $R_{\gamma\gamma}$ and $R_{Z\gamma}$, defined in Sec. IV. The projection of experimental measurements of the H boson branching fractions to 3000 fb $^{-1}$ of LHC data has been performed in Ref. [112]. In particular, Table 37 of this reference estimates $R_{\gamma\gamma} \simeq 1.00 \pm 0.05$ and $R_{Z\gamma} \simeq$ 1.00 ± 0.24 at 68% C.L. However, these measurements are estimated using the coupling modifier framework (κ -framework), where the tensor structures of interactions of the H boson and the kinematic distributions are assumed to be the same as in the SM. Though the kinematic distributions in decays $H \rightarrow \gamma \gamma$ and $Z\gamma$ are not affected by anomalous couplings, other aspects of the analyses, such as distributions of associated particles, would be affected. Nonetheless, one can use these estimates as optimistic expectations of constraints on $R_{\gamma\gamma}$ and $R_{Z\gamma}$ with anomalous contributions.

Relating the experimental constraints on $R_{\gamma\gamma}$ and $R_{Z\gamma}$ to constraints on $g_2^{\gamma\gamma}$, $g_4^{\gamma\gamma}$, $g_2^{Z\gamma}$, and $g_4^{Z\gamma}$ is not trivial, as various loop contributions are possible, as indicated in Eqs. (17) and (26). In particular, modifications of the H boson

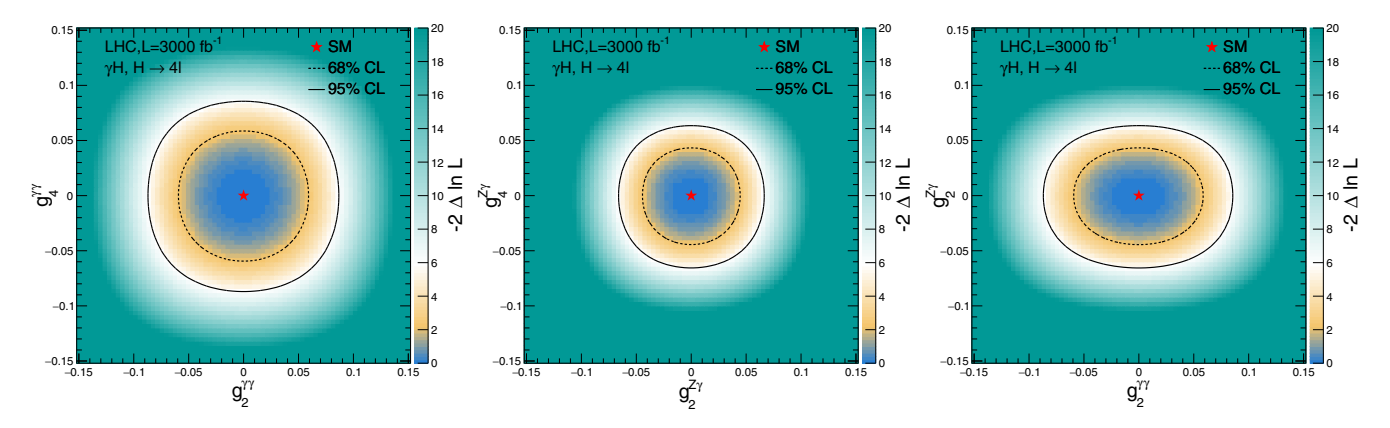


FIG. 13. Expected two-dimensional constraints from a simultaneous fit of $g_2^{\gamma\gamma}$, $g_4^{\gamma\gamma}$, $g_2^{Z\gamma}$, and $g_4^{Z\gamma}$ using the γH production channel.

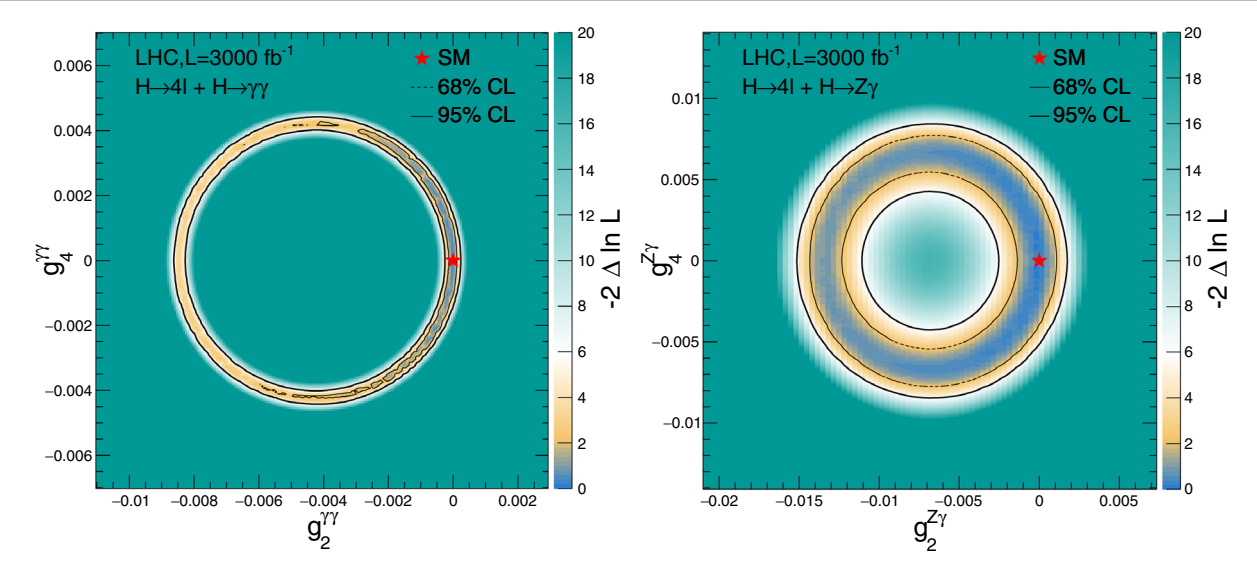


FIG. 14. Expected two-dimensional constraints on $(g_2^{\gamma\gamma}, g_4^{\gamma\gamma})$ (left), and $(g_2^{Z\gamma}, g_4^{Z\gamma})$ (right) using Eqs. (23) and (30) and the HL-LHC projection for experimental measurements of $R_{\gamma\gamma}$ and $R_{Z\gamma}$ from Ref. [112]. Inclusion of the $H \to 4\ell$ data with decay and production information helps in resolving degenerate solutions on a ring of a given radius.

couplings to fermions and W boson, which are the dominant SM contributions to the loop, cannot be disentangled from the effective pointlike couplings indicated with the κ_Q and $\tilde{\kappa}_Q$ couplings. The latter are related to $g_{2,4}^{\gamma\gamma,Z\gamma}$ with Q and R_Q in Eqs. (18) and (27). However, assuming that the H boson couplings to fermions and W boson can be constrained to high precision from other measurements, one can set those to SM values for the purpose of this comparison. In such a case, $R_{\gamma\gamma}$ and $R_{Z\gamma}$ could be expressed directly through the $g_{2,4}^{\gamma\gamma}$ and $g_{2,4}^{Z\gamma}$ couplings, respectively, without further complication, as shown in Eqs. (23) and (30).

With the above assumptions, the expected two-dimensional constraints on $(g_2^{\gamma\gamma},g_4^{\gamma\gamma})$ and on $(g_2^{Z\gamma},g_4^{Z\gamma})$ are circles in the 2D plane of the two couplings, as follows from Eqs. (23) and (30), respectively. All points on the circle of a given radius are equally likely, because one cannot distinguish between the CP-odd and CP-even couplings from the rate information alone. However, the addition of $H \to 4\ell$ decay and production information, discussed above, will help to resolve degenerate solutions, as shown in Fig. 14. The improvement from the inclusion of the $H \to 4\ell$ data is more visible in the case of the $H\gamma\gamma$ couplings. As we would expect, constraints from the $H \to \gamma\gamma$ and $Z\gamma$ rates are more restrictive than the constraints obtained from either decay or production information shown in Figs. 12 and 13.

As we reach precision on anomalous $H\gamma\gamma$ and $HZ\gamma$ couplings from the $H \to 4\ell$ decay and from VBF, VH, and γH production comparable to that from the $H \to \gamma\gamma$ and $Z\gamma$ decays, resolving the loop contributions in these production and decay processes will become important. This is similar to the discussion of $H \to \gamma\gamma$ and $Z\gamma$ in Sec. IV, but taking into account nontrivial q^2 -dependence affecting kinematic

distributions. This is equivalent to the NLO EW corrections discussed in Sec. V in application to the SM processes, but would require consideration of anomalous couplings.

VIII. SUMMARY

We have presented a study of electroweak production of the H boson in VBF and VH and its decay to two vector bosons, with a focus on the treatment of virtual loops of either SM particles or new states appearing in HVV interactions. The treatment of virtual photons has been illustrated with the JHU generator framework, and comparisons have been made to several other frameworks, including SMEFTsim using MadGraph5, HAWK, PROPHECY4F. A JHUGenLexicon program has been introduced for EFT parametrization and translation between frameworks. Overall, good agreement between the frameworks is found, including parametrization of EFT effects, once the sign conventions are matched, such as of the antisymmetric tensor $\varepsilon_{\mu\nu\rho\sigma}$ and the convariant derivative. The photon couplings appear to have a larger relative effect in decay compared to production, due to the dynamics of these processes. Nonetheless, the γH production topology appears interesting for isolating the photon couplings.

We have derived the scaling of the H boson production and decay rates with anomalous couplings, which are necessary for the total width calculations. From these, we also obtained the effective pointlike couplings which reproduce the $H \to gg$, $\gamma\gamma$, and $Z\gamma$ processes in the SM. We compared the effect of these couplings to the NLO EW corrections in the other processes with off-shell vector bosons. While the effects may be reproduced to within an order of magnitude, the effective couplings are not adequate for a careful modeling of the EW correction.

At the same time, however, the squared higher-order terms may become as important as linear terms at lower q^2 values of the virtual photons, something that is neglected in the NLO EW corrections. Subsequently, we make a proposal on how to handle singularities involving H boson decays to light fermions via photons. This procedure, based on matching amplitudes in the collinear limit, allows one to handle these singularities with efficient numerical evaluation. This approach can also incorporate the hadronic structure in decays to quarks using the experimentally measured quantities in low-energy processes.

We further make phenomenological observations on the special role of intermediate photons in analysis of LHC data in the EFT framework. Some of these features have been illustrated with projections for experimental measurements with the full LHC and HL-LHC datasets. The rates of the $H \to \gamma \gamma$ and $Z \gamma$ processes appear the most restrictive on the photon couplings, but cannot disentangle the CP-even and CP-odd couplings. We observe that the decay information $H \to 4\ell$ is more powerful in constraining the photon couplings than information in the VBF and VH production using the same H boson decay channel. However, these production channels, along with the γH production, can be analyzed using other H boson decays, with further gain in sensitivity to the photon couplings. The $H \to 4\ell$ channel can also be further optimized for the measurements of the photon couplings by relaxing the invariant mass and transverse momentum constraints on the leptons in analysis of LHC data. This will also require careful consideration of NLO EW effects in these processes, while including effects of anomalous contributions. Calculation of these effects will be required for precise analysis of HL-LHC data.

ACKNOWLEDGMENTS

This research is partially supported by the U.S. NSF under Grant No. PHY-2012584. Calculations reported in this paper were performed on the Maryland Advanced

Research Computing Center (MARCC). We thank our colleagues on the JHU event generator project for help and support, and in particular Rengi Pan, Ulascan Sarica, Yaofu Zhou, and Meng Xiao, and acknowledge the contributions of the CMS Collaboration colleagues to validation of the JHU event generator and the MELA project development. We thank Ritvik Gunturu and Valdis Slokenbergs for help with generating MC samples. We thank Marco Zaro, Fabio Maltoni, and Kentarou Mawatari for discussion of MadGraph sign conventions; Ilaria Brivio and Michael Trott for discussion of SMEFTsim; Adam Falkowski and Ken Mimasu for discussion of ROSETTA; Ansgar Denner, Stefan Dittmaier, and Alexander Mück for help with the PROPHECY4F and HAWK generators; Werner Bernreuther and Long Chen for discussion of loop calculations; Ian Low and Roberto Vega-Morales for discussion of analytical calculations; Andrew Gilbert and Jonathon Langford for discussion of EFT approaches on CMS. We also thank other members of the LHC Higgs and EFT Working Groups for stimulating discussions.

APPENDIX A: RELATIVE CONTRIBUTIONS OF OPERATORS TO H BOSON PROCESSES ON THE LHC

In the following, we investigate the relative contributions of the operators listed in Table I to the VBF, VH, and $H \rightarrow VV \rightarrow 4\ell$ processes. We obtain these contributions of individual terms in the mass-eigenstate basis relative to the overall cross section of a single operator in the Warsaw basis, excluding the SM coupling, and relative to the SM cross section alone $(\sigma/\sigma_{\rm SM})$. The results are shown in Tables IV–VIII, where the relative contributions are shown separately for the $H \rightarrow VV \rightarrow 4\ell$, VBF, $q\bar{q}$ or $gg \rightarrow V(\rightarrow \ell^+\ell^-)H$, and γH processes. The fractions do not necessarily add up to 1 due to interference effects. The ratio to the SM expectation is shown for $C_{HX}=1$. As discussed in more detail in Secs. IV and VI, the presence of collinear singularities requires a special treatment of the

TABLE IV. Relative contributions of the individual terms in the mass-eigenstate amplitude to a single operator C_{HX} in the Warsaw basis expressed as a fraction of the gg $\to H \to 4\ell$ cross section. The SM contribution is excluded from the HVV coupling, and the cross section ratio to the SM expectation (σ/σ_{SM}) is shown for $C_{HX}=1$ in the first column. The contributions to the $H \to 4\ell$ process are shown with the requirement $m_{\ell\ell}>1$ GeV.

	$\sigma/\sigma_{ m SM}$	$\delta g_1^{ZZ} = \delta g_1^{WW}$	κ_1^{ZZ}	g_2^{ZZ}	$g_2^{Z\gamma}$	$g_2^{\gamma\gamma}$	g_4^{ZZ}	$g_4^{Z\gamma}$	$g_4^{\gamma\gamma}$	$\kappa_2^{Z\gamma}$	κ_1^{WW}	g_2^{WW}	g_4^{WW}
$C_{H\square}$	0.004	1	0	0	0	0	0	0	0	0	0	0	0
C_{HD}	0.017	1.078	0.068	0	0	0	0	0	0	0.486	0	0	0
C_{HW}	0.635	0	0	0.00117	0.685	0.238	0	0	0	0	0	0	0
C_{HWB}	0.781	0.007	0.001	0.00029	0.268	0.632	0	0	0	0.018	0	0	0
C_{HB}	2.215	0	0	0.00003	0.243	0.759	0	0	0	0	0	0	0
$C_{H ilde{W}}$	0.579	0	0	0	0	0	0.00052	0.713	0.286	0	0	0	0
$C_{H ilde{W}B}$	0.749	0	0	0	0	0	0.00012	0.239	0.683	0	0	0	0
$C_{H ilde{B}}$	2.196	0	0	0	0	0	0.00001	0.194	0.720	0	0	0	0

TABLE V. Relative contributions, as in Table IV, to the cross section of the VBF process, with the requirement $q_V^2 > 1 \text{ GeV}^2$.

	$\sigma/\sigma_{ m SM}$	$\delta g_1^{\rm ZZ} = \delta g_1^{\rm WW}$	κ_1^{ZZ}	g_2^{ZZ}	$g_2^{Z\gamma}$	$g_2^{\gamma\gamma}$	g_4^{ZZ}	$g_4^{Z\gamma}$	$g_4^{\gamma\gamma}$	$\kappa_2^{Z\gamma}$	κ_1^{WW}	g_2^{WW}	g_4^{WW}
$\overline{C_{H\square}}$	0.004	1	0	0	0	0	0	0	0	0	0	0	0
C_{HD}	0.170	0.105	0.081	0	0	0	0	0	0	0.154	0.572	0	0
C_{HW}	0.052	0	0	0.159	0.196	0.059	0	0	0	0	0	0.839	0
C_{HWB}	0.086	0.067	0.086	0.030	0.046	0.115	0	0	0	0.531	0.059	0	0
C_{HB}	0.063	0	0	0.012	0.159	0.522	0	0	0	0	0	0	0
$C_{H ilde{W}}$	0.043	0	0	0	0	0	0.153	0.207	0.066	0	0	0	0.811
$C_{H ilde{W}B}$	0.012	0	0	0	0	0	0.170	0.304	0.831	0	0	0	0
$C_{H ilde{B}}$	0.059	0	0	0	0	0	0.010	0.156	0.520	0	0	0	0

TABLE VI. Relative contributions, as in Table IV, to the cross section of the $q\bar{q} \to V(\to \ell^+\ell^-)H$ process, with the requirement $m_{\ell\ell} > 1$ GeV.

	$\sigma/\sigma_{ m SM}$	$\delta g_1^{ZZ} = \delta g_1^{WW}$	κ_1^{ZZ}	g_2^{ZZ}	$g_2^{Z\gamma}$	$g_2^{\gamma\gamma}$	g_4^{ZZ}	$g_4^{Z\gamma}$	$g_4^{\gamma\gamma}$	$\kappa_2^{Z\gamma}$	κ_1^{WW}	g_2^{WW}	g_4^{WW}
$C_{H\square}$	0.004	1	0	0	0	0	0	0	0	0	0	0	0
C_{HD}	0.949	0.019	0.655	0	0	0	0	0	0	1.026	0	0	0
C_{HW}	0.154	0	0	1.087	0.294	0.017	0	0	0	0	0	0	0
C_{HWB}	2.265	0.003	0.151	0.022	0.008	0.004	0	0	0	0.774	0	0	0
C_{HB}	0.125	0	0	0.125	0.366	0.232	0	0	0	0	0	0	0
$C_{H ilde{W}}$	0.097	0	0	0	0	0	1.044	0.330	0.023	0	0	0	0
$C_{H\tilde{W}B}$	0.057	0	0	0	0	0	0.536	0.218	0.125	0	0	0	0
$C_{H\tilde{B}}$	0.090	0	0	0	0	0	0.106	0.353	0.263	0	0	0	0

TABLE VII. Relative contributions, as in Table IV, to the cross section of the gg $\to Z(\to \ell^+\ell^-)H$ process, with the requirement $m_{\ell\ell} > 1$ GeV.

	$\sigma/\sigma_{ m SM}$	$\delta g_1^{ZZ} = \delta g_1^{WW}$	κ_1^{ZZ}	g_2^{ZZ}	$g_2^{Z\gamma}$	$g_2^{\gamma\gamma}$	g_4^{ZZ}	$g_4^{Z\gamma}$	$g_4^{\gamma\gamma}$	$\kappa_2^{Z\gamma}$	κ_1^{WW}	g_2^{WW}	g_4^{WW}
$\overline{C_{H\square}}$	0.009	1	0	0	0	0	0	0	0	0	0	0	0
C_{HD}	8.055	0.006	1.100	0	0	0	0	0	0	0	0	0	0
C_{HW}	0	0	0	0	0	0	0	0	0	0	0	0	0
C_{HWB}	4.495	0.003	1.066	0	0	0	0	0	0	0	0	0	0
C_{HB}	0	0	0	0	0	0	0	0	0	0	0	0	0
$C_{H ilde{W}}$	0	0	0	0	0	0	0	0	0	0	0	0	0
$C_{H ilde{W}B}$	0	0	0	0	0	0	0	0	0	0	0	0	0
$C_{H\tilde{B}}$	0	0	0	0	0	0	0	0	0	0	0	0	0

TABLE VIII. Relative contributions, as in Table IV, to the cross section of the $q\bar{q} \to \gamma H$ process.

	$\sigma/\sigma_{ m SM}^{\gamma H}$	$\delta g_1^{ZZ} = \delta g_1^{WW}$	κ_1^{ZZ}	g_2^{ZZ}	$g_2^{Z\gamma}$	$g_2^{\gamma\gamma}$	g_4^{ZZ}	$g_4^{Z\gamma}$	$g_4^{\gamma\gamma}$	$\kappa_2^{Z\gamma}$	κ_1^{WW}	g_2^{WW}	g_4^{WW}
$C_{H\square}$	0	0	0	0	0	0	0	0	0	0	0	0	0
C_{HD}	0	0	0	0	0	0	0	0	0	0	0	0	0
C_{HW}	60.3	0	0	0	1.190	0.197	0	0	0	0	0	0	0
C_{HWB}	41.1	0	0	0	0.688	0.956	0	0	0	0	0	0	0
C_{HB}	271.3	0	0	0	0.260	0.472	0	0	0	0	0	0	0
$C_{H ilde{W}}$	60.1	0	0	0	0	0	0	1.182	0.198	0	0	0	0
$C_{H ilde{W}B}$	41.7	0	0	0	0	0	0	0.677	0.930	0	0	0	0
$C_{H\tilde{B}}$	273.9	0	0	0	0	0	0	0.263	0.472	0	0	0	0

low- q_V^2 of the gauge bosons, and in the study in this Appendix we choose to apply a requirement $q_V^2 > 1 \text{ GeV}^2$. The results of this study are discussed in Sec. III.

APPENDIX B: DERIVATION OF THE COLLINEAR APPROXIMATION TO THE H BOSON WIDTH WITH INTERMEDIATE PHOTONS

1. Phase space

The general H boson decay phase space reads

$$dPS^{(N)}(E^2, m_1^2, ..., m_N^2)$$

$$= (2\pi)^{4-3N} \left[\prod_{i=1}^{N} d^4 p_i \delta(p_i^2 - m_i^2) \theta(p_i^0) \right] \delta^{(4)} \left(p_H - \sum_{i=1}^{N} p_i \right). \tag{B1}$$

We rewrite the four-particle phase space in Eq. (B1)

$$\int dPS^{(4)}(m_H^2, m_1^2, m_2^2, m_3^2, m_4^2)$$

$$= (2\pi)^{-8} \int \left[\prod_{i=1}^4 d^4 p_i \delta(p_i^2 - m_i^2) \theta(p_i^0) \right]$$

$$\times \delta^{(4)}(p_H - p_1 - p_2 - p_3 - p_4), \tag{B2}$$

by inserting the additional integrals

$$1 = \int d^4 p_{ij} \delta^{(4)}(p_{ij} - p_i - p_j),$$
 (B3)

$$1 = \int_{q_{ij\,\text{min}}}^{q_{ij,\text{max}}} \mathrm{d}q_{ij}^2 \delta(q_{ij}^2 - p_{ij}^2), \tag{B4}$$

for (ij) = (12) and (ij) = (34). This yields

$$\begin{split} \int \mathrm{dPS}^{(4)}(\ldots) &= (2\pi)^{-6} \int_{q_{12,\mathrm{min}}^2}^{q_{12,\mathrm{max}}^2} \frac{\mathrm{d}q_{12}^2}{2\pi} \int_{q_{34,\mathrm{min}}^2}^{q_{34,\mathrm{max}}^2} \frac{\mathrm{d}q_{34}^2}{2\pi} \mathrm{d}^4 p_{12} \delta(p_{12}^2 - q_{12}^2) \mathrm{d}^4 p_{34} \delta(p_{34}^2 - q_{34}^2) \delta^{(4)}(p_H - p_{12} - p_{34}) \\ &\times \int \prod_{(ij)=(12),(34)} \mathrm{d}^4 p_i \mathrm{d}^4 p_j \delta(p_i^2 - m_i^2) \delta(p_j^2 - m_j^2) \theta(p_i^0) \theta(p_j^0) \delta^{(4)}(p_{ij} - p_i - p_j) \\ &= \int_{q_{12,\mathrm{min}}^2}^{q_{12,\mathrm{max}}^2} \frac{\mathrm{d}q_{12}^2}{2\pi} \int_{q_{34,\mathrm{min}}^2}^{q_{34,\mathrm{max}}^2} \frac{\mathrm{d}q_{34}^2}{2\pi} \int \mathrm{dPS}^{(2)}(m_H^2, q_{12}^2, q_{34}^2) \mathrm{dPS}^{(2)}(q_{12}^2, m_1^2, m_2^2) \mathrm{dPS}^{(2)}(q_{34}^2, m_3^2, m_4^2), \end{split} \tag{B5}$$

where $q_{ij,\text{min}}^2 = 4m_i^2$, $q_{12,\text{max}}^2 = m_H^2$, and $q_{34,\text{max}}^2 = (m_H - \sqrt{q_{12}^2})^2$. In this form, the two integrals over q_{ij}^2 directly correspond to the V and V' squared invariant masses of the matrix element $\mathcal{M}_{H \to 4f}$. This will be useful later.

In case of identical fermions, it is useful to symmetrize the phase space in the last line of Eq. (B5) because the matrix element has resonances not only in q_{12}^2 and q_{34}^2 but also in q_{14}^2 and q_{32}^2 , i.e., $\mathcal{M} = A(1234) + A(1432)$. Therefore, in practice we run the numerical simulation using

$$\int dPS^{(4)}(...) = \frac{1}{2} [(Eq. (B5)) + (Eq. (B5))|_{2\leftrightarrow 4}].$$
 (B6)

In this write up, however, we do not symmetrize the phase space for clarity of presentation. The analytic result is of course equivalent because

$$\begin{split} &\frac{1}{2}[(\text{Eq. (B5)}) + (\text{Eq. (B5)})|_{2\leftrightarrow 4}] \times |A(1234) + A(1432)|^2 \\ &= (\text{Eq. (B5)}) \times |\mathcal{M}|^2. \end{split} \tag{B7}$$

In a similar fashion, we rewrite the three-particle phase space in Eq. (B1) as

$$\int dPS^{(3)}(...) = \int_{q_{12,\text{min}}^2}^{q_{12,\text{max}}^2} \frac{dq_{12}^2}{2\pi} \int dPS^{(2)}(m_H^2, q_{12}^2, 0) \times dPS^{(2)}(q_{12}^2, m_1^2, m_2^2),$$
(B8)

where the integration boundaries are $q_{12,\mathrm{min}}^2 = 4m_1^2$ and $q_{12,\mathrm{max}}^2 = m_H^2$.

2. Collinear approximation

Collinear factorization properties of a general process with leptons $(f = e, \mu, \tau)$ yields

$$\int dPS^{(N)} |\mathcal{M}_{X+\ell\bar{\ell}}|^{2} \xrightarrow{(p_{\ell}+p_{\ell})^{2} \ll \mu^{2}} \frac{\alpha}{2\pi} S_{\ell}(\mu^{2})$$

$$\times \int dPS^{(N-1)} |\mathcal{M}_{X+\gamma}|^{2} + \mathcal{O}(\mu^{2}/\hat{s}), \tag{B9}$$

where $\hat{s} \gg \mu^2$ is a typical momentum scale of the process and [62]

$$\begin{split} S_{\ell}(\mu^2) &= \int_0^1 \mathrm{d}x \bigg[(x^2 + (1-x)^2) \log \bigg(\frac{\mu^2}{m_{\ell}^2} x (1-x) \bigg) + 2x (1-x) \bigg] \\ &= \frac{2}{3} \log \bigg(\frac{\mu^2}{m_{\ell}^2} \bigg) - \frac{10}{9} \,. \end{split} \tag{B10}$$

In case of hadronic final states $\gamma^* \rightarrow jj$ Eq. (B9) becomes

$$\int dPS^{(N)} |\mathcal{M}_{X+jj}|^2 \xrightarrow{(p_q + p_{\bar{q}})^2 \ll \mu^2} \frac{\alpha}{2\pi} S_{\text{had}}(\mu^2)$$

$$\times \int dPS^{(N-1)} |\mathcal{M}_{X+\gamma}|^2 + \mathcal{O}(\mu^2/\hat{s}), \tag{B11}$$

where $S_{\text{had}}(\mu^2)$ contains nonperturbative contributions and is closely related to $F_{\text{had}}(\mu^2)$ in Ref. [62]. It can be written as

$$S_{\text{had}}(\mu^2) = \frac{22}{9} \log \left(\frac{\mu^2}{M_Z^2} \right) + 2\pi \frac{\Delta \alpha_{\text{had}}^{(5)}(M_Z^2)}{\alpha}.$$
 (B12)

 $\Delta\alpha_{\rm had}^{(5)}(s)$ is the hadronic contribution of the shift in the running electromagnetic coupling (with five active quark flavors) in $\alpha(s) = \alpha(0)/(1-\Delta\alpha(s))$ and is measured to be $\Delta\alpha_{\rm had}^{(5)}(M_Z^2) = (276.11 \pm 1.11) \times 10^{-4}$ [100,101].

3. Collinear approximation applied to $H \rightarrow 2\ell\gamma$

We split the invariant mass integration in Eq. (B8)

$$\left(\int_{q_{12,\text{min}}^2}^{\mu^2} \mathrm{d}q_{12}^2 + \int_{\mu^2}^{q_{12,\text{max}}^2} \mathrm{d}q_{12}^2\right) \tag{B13}$$

and define two regions I and II, respectively. This yields region I where the collinear approximation for intermediate photons can be applied

$$\Gamma_{H \to \gamma^* \gamma \to 2\ell \gamma}^{I}(\mu^2) = \frac{1}{2m_H} \int_{q_{12,\text{min}}^2}^{\mu^2} \frac{q_{12}^2}{2\pi} \int dPS^{(2)}(m_H^2, q_{12}^2, 0) dPS^{(2)}(q_{12}^2, m_1^2, m_2^2) |\mathcal{M}_{H \to \gamma^* \gamma \to 2\ell \gamma}|^2
= \frac{1}{2m_H} \frac{\alpha}{2\pi} S_{\ell}(\mu^2) \int dPS^{(2)}(m_H^2, 0, 0) |\mathcal{M}_{H \to \gamma \gamma}|^2 + \mathcal{O}(\mu^2/\hat{s})
= \frac{\alpha}{2\pi} S_{\ell}(\mu^2) (2_{\gamma \gamma}) \Gamma_{H \to \gamma \gamma} + \mathcal{O}(\mu^2/\hat{s}).$$
(B14)

For intermediate Z bosons in region I, we just keep it as it is

$$\Gamma^I_{H\to Z^*\gamma\to 2\ell\gamma}(\mu^2) = \Gamma_{H\to Z^*\gamma\to 2\ell\gamma}|_{q^2_{12}<\mu^2}. \tag{B15}$$

The interference between γ^* and Z^* states is zero in the collinear approximation in region I. In region II, the collinear approximation for intermediate photons is not applied and includes intermediate photons and Zs and their interference

$$\begin{split} \Gamma^{\rm II}_{H\to 2\ell\gamma}(\mu^2) = & \frac{1}{2m_H} \int_{\mu^2}^{q_{12,\rm max}^2} \frac{\mathrm{d}q_{12}^2}{2\pi} \int \mathrm{dPS}^{(2)}(m_H^2, q_{12}^2, 0) \\ & \times \mathrm{dPS}^{(2)}(q_{12}^2, m_1^2, m_2^2) |\mathcal{M}_{H\to 2\ell\gamma}|^2 \\ = & \Gamma_{H\to 2\ell\gamma}|_{q_{12}^2 \ge \mu^2}. \end{split} \tag{B16}$$

Hence, we end up with the sum of the above contributions

$$\begin{split} \Gamma_{H \to 2\ell\gamma} &= \Gamma^{\rm I}_{H \to \gamma^* \gamma \to 2\ell \gamma}(\mu^2) + \Gamma^{\rm II}_{H \to \gamma^* \gamma \to 2\ell \gamma}(\mu^2) \\ &+ \Gamma^{\rm I}_{H \to Z^* \gamma \to 2\ell \gamma}(\mu^2). \end{split} \tag{B17}$$

4. Collinear approximation applied to $H \rightarrow 4\ell$

Now, we use the phase space parametrization in Eq. (B5) and split the two q_{ij}^2 integrations into a low-mass and high-mass region, which are separated by μ^2 . Hence, we write it as

$$\left(\int_{q_{12,\text{min}}^2}^{\mu^2} dq_{12}^2 + \int_{\mu^2}^{q_{12,\text{max}}^2} dq_{12}^2 \right) \\
\times \left(\int_{q_{34,\text{min}}^2}^{\mu^2} dq_{34}^2 + \int_{\mu^2}^{q_{34,\text{max}}^2} dq_{34}^2 \right), \tag{B18}$$

resulting in four regions I–IV. If we choose μ^2 such that $q_{ij,\text{min}}^2 \ll \mu^2 \ll \hat{s}$ then we can apply the collinear approximation of Eq. (B9) in the respective sectors.⁵ Let us start with region I, where $q_{12}^2 \leq \mu^2$ and $q_{34}^2 > \mu^2$

⁵We assume that in the collinear regions the matrix element is dominated by γ^* exchange such that we can neglect Z^* exchange.

$$\begin{split} \Gamma^{\rm I}_{H\to 2\ell'2\ell'}(\mu^2) &= \frac{1}{2m_H} \frac{1}{(4_{\ell\ell'})} \int_{q^2_{12,\rm min}}^{\mu^2} \frac{\mathrm{d}q^2_{12}}{2\pi} \int_{\mu^2}^{q^2_{34,\rm max}} \frac{\mathrm{d}q^2_{34}}{2\pi} \int \mathrm{dPS}^{(2)}(m_H^2, q^2_{12}, q^2_{34}) \, \mathrm{dPS}^{(2)}(q^2_{12}, m^2_1, m^2_2) \\ &\times \mathrm{dPS}^{(2)}(q^2_{34}, m^2_3, m^2_4) |\mathcal{M}_{H\to 2\ell'2\ell'}|^2 \\ &= \frac{1}{2m_H} \frac{1}{(4_{\ell\ell'})} \frac{\alpha}{2\pi} S_{\ell}(\mu^2) \int_{\mu^2}^{q^2_{34,\rm max}} \frac{\mathrm{d}q^2_{34}}{2\pi} \int \mathrm{dPS}^{(2)}(m_H^2, 0, q^2_{34}) \mathrm{dPS}^{(2)}(q^2_{34}, m^2_3, m^2_4) |\mathcal{M}_{H\to \gamma^2\ell'}|^2 + \mathcal{O}(\mu^2/\hat{s}) \\ &+ \frac{1}{2m_H} \frac{1}{(4_{\ell\ell'})} \int_{q^2_{12,\rm min}}^{\mu^2} \frac{\mathrm{d}q^2_{12}}{2\pi} \int_{\mu^2}^{q^2_{34,\rm max}} \frac{\mathrm{d}q^2_{34}}{2\pi} \int \mathrm{dPS}^{(2)}(m_H^2, q^2_{12}, q^2_{34}) \, \mathrm{dPS}^{(2)}(q^2_{12}, m^2_1, m^2_2) \\ &\times \mathrm{dPS}^{(2)}(q^2_{34}, m^2_3, m^2_4) |\mathcal{M}_{H\to Z^*(\to 2\ell') + Z^*/\gamma^*(\to 2\ell')}|^2 \\ &= \frac{\alpha}{2\pi} \frac{1}{(2_{\ell\ell'})} S_{\ell}(\mu^2) \Gamma_{H\to \gamma^2\ell'} \Big|_{q^2_{34} \ge \mu^2} + \mathcal{O}(\mu^2/\hat{s}) + \Gamma_{H\to Z^*(\to 2\ell') + Z^*/\gamma^*(\to 2\ell')} \Big|_{q^2_{12} < \mu^2, q^2_{34} \ge \mu^2}. \end{split} \tag{B19}$$

In a completely analog way, we find region II with $q_{12}^2 > \mu^2$ and $q_{34}^2 \le \mu^2$

$$\begin{split} \Gamma^{\mathrm{II}}_{H \to 2\ell 2\ell'}(\mu^2) &= \frac{1}{2m_H} \frac{1}{(4_{\ell\ell'})} \int_{\mu^2}^{q_{12,\mathrm{max}}^2} \frac{\mathrm{d}q_{12}^2}{2\pi} \int_{q_{34,\mathrm{min}}^2}^{\mu^2} \frac{\mathrm{d}q_{34}^2}{2\pi} \int \mathrm{dPS}^{(2)}(m_H^2, q_{12}^2, q_{34}^2) \, \mathrm{dPS}^{(2)}(q_{12}^2, m_1^2, m_2^2) \\ &\quad \times \mathrm{dPS}^{(2)}(q_{34}^2, m_3^2, m_4^2) |\mathcal{M}_{H \to 2\ell 2\ell'}|^2 \\ &= \frac{\alpha}{2\pi} \frac{1}{(2_{\ell\ell'})} S_{\ell'}(\mu^2) \Gamma_{H \to 2\ell\gamma} \bigg|_{q_{12}^2 \ge \mu^2} + \mathcal{O}(\mu^2/\hat{s}) + \Gamma_{H \to Z^*/\gamma^*(\to 2\ell') + Z^*(\to 2\ell')} \bigg|_{q_{12}^2 \ge \mu^2, q_{34}^2 < \mu^2}. \end{split} \tag{B20}$$

The region III contains the case where both, q_{12}^2 and q_{34}^2 , are smaller than μ^2

$$\begin{split} \Gamma^{\text{III}}_{H \to 2\ell' 2\ell'}(\mu^2) &= \frac{1}{2m_H} \frac{1}{(4_{\ell\ell'})} \int_{q^2_{12,\text{min}}}^{\mu^2} \frac{\mathrm{d}q^2_{12}}{2\pi} \int_{q^2_{34,\text{min}}}^{\mu^2} \frac{\mathrm{d}q^2_{34}}{2\pi} \int \mathrm{dPS}^{(2)}(m_H^2, q^2_{12}, q^2_{34}) \, \mathrm{dPS}^{(2)}(q^2_{12}, m^2_1, m^2_2) \\ &\times \mathrm{dPS}^{(2)}(q^2_{34}, m^2_3, m^2_4) |\mathcal{M}_{H \to 2\ell' 2\ell'}|^2 \\ &= \frac{1}{2m_H} \frac{1}{(2_{\ell\ell'})} \left(\frac{\alpha}{2\pi}\right)^2 S_{\ell}(\mu^2) S_{\ell'}(\mu^2) \int \mathrm{dPS}^{(2)}(m_H^2, 0, 0) |\mathcal{M}_{H \to \gamma\gamma}|^2 + \mathcal{O}(\mu^2/\hat{s}) \\ &+ \frac{1}{2m_H} \frac{1}{(4_{\ell\ell'})} \int_{q^2_{12,\text{min}}}^{\mu^2} \frac{\mathrm{d}q^2_{12}}{2\pi} \int_{q^2_{34,\text{min}}}^{\mu^2} \frac{\mathrm{d}q^2_{34}}{2\pi} \int \mathrm{dPS}^{(2)}(m_H^2, q^2_{12}, q^2_{34}) \, \mathrm{dPS}^{(2)}(q^2_{12}, m^2_1, m^2_2) \\ &\times \mathrm{dPS}^{(2)}(q^2_{34}, m^2_3, m^2_4) |\mathcal{M}_{H \to Z^*Z^* \to 2\ell' 2\ell'}|^2 \\ &= \left(\frac{\alpha}{2\pi}\right)^2 \frac{(2_{\gamma\gamma})}{(2_{\ell\ell'})} S_{\ell}(\mu^2) S_{\ell'}(\mu^2) \Gamma_{H \to \gamma\gamma} + \mathcal{O}(\mu^2/\hat{s}) + \Gamma_{H \to Z^*Z^* \to 2\ell' 2\ell'} \right|_{q^2_{13} < u^2, q^2_{23} < u^2}. \end{split} \tag{B21}$$

Region IV contains the case where both, q_{12}^2 and q_{34}^2 , are larger than μ^2 . Therefore, no collinear approximation is applied

$$\begin{split} \Gamma^{\text{IV}}_{H \to 2\ell 2\ell'}(\mu^2) &= \frac{1}{2m_H} \frac{1}{(4_{\ell\ell'})} \int_{\mu^2}^{q_{12,\text{max}}^2} \frac{\mathrm{d}q_{12}^2}{2\pi} \int_{\mu^2}^{q_{34,\text{max}}^2} \frac{\mathrm{d}q_{34}^2}{2\pi} \int \mathrm{dPS}^{(2)}(m_H^2, q_{12}^2, q_{34}^2) \mathrm{dPS}^{(2)}(q_{12}^2, m_1^2, m_2^2) \\ &\quad \times \mathrm{dPS}^{(2)}(q_{34}^2, m_3^2, m_4^2) |\mathcal{M}_{H \to 2\ell'2\ell'}|^2 \\ &= \Gamma_{H \to 2\ell'2\ell'} |_{q_{12}^2 \ge \mu^2, q_{34}^2 \ge \mu^2} \end{split} \tag{B22}$$

Finally, we can write Eq. (33) as

$$\Gamma_{H\to2\ell'2\ell'} = \Gamma^{\mathrm{I}}_{H\to2\ell'2\ell'}(\mu^2) + \Gamma^{\mathrm{II}}_{H\to2\ell'2\ell'}(\mu^2) + \Gamma^{\mathrm{III}}_{H\to2\ell'2\ell'}(\mu^2) + \Gamma^{\mathrm{IV}}_{H\to2\ell'2\ell'}(\mu^2). \tag{B23}$$

Note that the left-hand side is independent of the arbitrary value μ , as long as $m_f^2 \ll \mu^2 \ll M_H^2$ is fulfilled. It is a nice feature that the anomalous couplings don't have to be made explicit in the above derivation. They are always contained in the partial widths $\Gamma_{H\to 4\ell}$, $\Gamma_{H\to 2\ell+\gamma}$, and $\Gamma_{H\to \gamma\gamma}$.

5. Decays to quarks

The derivations in the previous Secs. B 4 and B 3 remain valid, if we sum over all five light quarks and replace $S_{\ell}(\mu^2) \to S_{had}(\mu^2)$.

- [1] ATLAS Collaboration, Observation of a new particle in the search for the Standard Model Higgs boson with the ATLAS detector at the LHC, Phys. Lett. B **716**, 1 (2012).
- [2] CMS Collaboration, Observation of a new boson at a mass of 125 GeV with the CMS experiment at the LHC, Phys. Lett. B **716**, 30 (2012).
- [3] CMS Collaboration, Study of the Mass and Spin-Parity of the Higgs Boson Candidate via Its Decays to Z Boson Pairs, Phys. Rev. Lett. 110, 081803 (2013).
- [4] C. A. Nelson, Correlation between decay planes in Higgs-boson decays into a W pair (into a Z pair), Phys. Rev. D **37**, 1220 (1988).
- [5] A. Soni and R. M. Xu, Probing CP violation via Higgs decays to four leptons, Phys. Rev. D 48, 5259 (1993).
- [6] D. Chang, W.-Y. Keung, and I. Phillips, CP odd correlation in the decay of neutral Higgs boson into ZZ, W⁺W⁻, or tt̄, Phys. Rev. D 48, 3225 (1993).
- [7] V. D. Barger, K. Cheung, A. Djouadi, B. A. Kniehl, and P. M. Zerwas, Higgs bosons: Intermediate mass range at e^+e^- colliders, Phys. Rev. D **49**, 79 (1994).
- [8] T. Arens and L. M. Sehgal, Energy spectra and energy correlations in the decay $H \to ZZ \to \mu^+\mu^-\mu^+\mu^-$, Z. Phys. C **66**, 89 (1995).
- [9] S. Bar-Shalom, D. Atwood, G. Eilam, R. R. Mendel, and A. Soni, Large tree level CP violation in $e^+e^- \rightarrow t\bar{t}H^0$ in the two Higgs doublet model, Phys. Rev. D **53**, 1162 (1996).
- [10] J. F. Gunion and X.-G. He, Determining the *CP* Nature of a Neutral Higgs Boson at the LHC, Phys. Rev. Lett. **76**, 4468 (1996).
- [11] T. Han and J. Jiang, CP violating ZH coupling at e^+e^- linear colliders, Phys. Rev. D **63**, 096007 (2001).
- [12] T. Plehn, D. L. Rainwater, and D. Zeppenfeld, Determining the Structure of Higgs Couplings at the LHC, Phys. Rev. Lett. 88, 051801 (2002).
- [13] S. Y. Choi, D. J. Miller, M. M. Mühlleitner, and P. M. Zerwas, Identifying the Higgs spin and parity in decays to Z pairs, Phys. Lett. B **553**, 61 (2003).
- [14] C. P. Buszello, I. Fleck, P. Marquard, and J. J. van der Bij, Prospective analysis of spin- and *CP*-sensitive variables in $H \to ZZ \to \ell_1^+ \ell_1^- \ell_2^+ \ell_2^-$ at the LHC, Eur. Phys. J. C **32**, 209 (2004).
- [15] V. Hankele, G. Klamke, D. Zeppenfeld, and T. Figy, Anomalous Higgs boson couplings in vector boson fusion at the CERN LHC, Phys. Rev. D 74, 095001 (2006).
- [16] E. Accomando et al., Proceedings of the 1st Workshop on CP Studies and Non-standard Higgs Physics, CERN,

- Geneva, Switzerland, edited by E. Accomando et al. (CERN, Geneva, Switzerland, 2006), 10.5170/CERN-2006-009.
- [17] R. M. Godbole, D. J. Miller, and M. M. Mühlleitner, Aspects of *CP* violation in the HZZ coupling at the LHC, J. High Energy Phys. 12 (2007) 031.
- [18] K. Hagiwara, Q. Li, and K. Mawatari, Jet angular correlation in vector-boson fusion processes at hadron colliders, J. High Energy Phys. 07 (2009) 101.
- [19] Y. Gao, A. V. Gritsan, Z. Guo, K. Melnikov, M. Schulze, and N. V. Tran, Spin determination of single-produced resonances at hadron colliders, Phys. Rev. D 81, 075022 (2010).
- [20] A. De Rújula, J. Lykken, M. Pierini, C. Rogan, and M. Spiropulu, Higgs look-alikes at the LHC, Phys. Rev. D 82, 013003 (2010).
- [21] N. D. Christensen, T. Han, and Y. Li, Testing CP violation in ZZH interactions at the LHC, Phys. Lett. B 693, 28 (2010).
- [22] J. S. Gainer, K. Kumar, I. Low, and R. Vega-Morales, Improving the sensitivity of Higgs boson searches in the golden channel, J. High Energy Phys. 11 (2011) 027.
- [23] S. Bolognesi, Y. Gao, A. V. Gritsan, K. Melnikov, M. Schulze, N. V. Tran, and A. Whitbeck, Spin and parity of a single-produced resonance at the LHC, Phys. Rev. D 86, 095031 (2012).
- [24] J. Ellis, D. S. Hwang, V. Sanz, and T. You, A fast track towards the 'Higgs' spin and parity, J. High Energy Phys. 11 (2012) 134.
- [25] Y. Chen, N. Tran, and R. Vega-Morales, Scrutinizing the Higgs signal and background in the $2 e^2 \mu$ golden channel, J. High Energy Phys. 01 (2013) 182.
- [26] J. S. Gainer, J. Lykken, K. T. Matchev, S. Mrenna, and M. Park, Geolocating the Higgs Boson Candidate at the LHC, Phys. Rev. Lett. 111, 041801 (2013).
- [27] P. Artoisenet *et al.*, A framework for Higgs characterisation, J. High Energy Phys. 11 (2013) 043.
- [28] I. Anderson *et al.*, Constraining anomalous HVV interactions at proton and lepton colliders, Phys. Rev. D 89, 035007 (2014).
- [29] M. Chen, T. Cheng, J. S. Gainer, A. Korytov, K. T. Matchev, P. Milenovic, G. Mitselmakher, M. Park, A. Rinkevicius, and M. Snowball, Role of interference in unraveling the ZZ couplings of the newly discovered boson at the LHC, Phys. Rev. D 89, 034002 (2014).
- [30] Y. Chen and R. Vega-Morales, Extracting effective Higgs couplings in the golden channel, J. High Energy Phys. 04 (2014) 057.

- [31] J. S. Gainer, J. Lykken, K. T. Matchev, S. Mrenna, and M. Park, Beyond geolocating: Constraining higher dimensional operators in $H \rightarrow 4\ell$ with off-shell production and more, Phys. Rev. D **91**, 035011 (2015).
- [32] M. Gonzalez-Alonso, A. Greljo, G. Isidori, and D. Marzocca, Pseudo-observables in Higgs decays, Eur. Phys. J. C 75, 128 (2015).
- [33] M. J. Dolan, P. Harris, M. Jankowiak, and M. Spannowsky, Constraining *CP*-violating Higgs sectors at the LHC using gluon fusion, Phys. Rev. D **90**, 073008 (2014).
- [34] F. Demartin, F. Maltoni, K. Mawatari, B. Page, and M. Zaro, Higgs characterisation at NLO in QCD: *CP* properties of the top-quark Yukawa interaction, Eur. Phys. J. C 74, 3065 (2014).
- [35] Y. Chen, R. Harnik, and R. Vega-Morales, Probing the Higgs Couplings to Photons in $H \to 4\ell$ at the LHC, Phys. Rev. Lett. **113**, 191801 (2014).
- [36] M. R. Buckley and D. Goncalves, Boosting the Direct *CP* Measurement of the Higgs-Top Coupling, Phys. Rev. Lett. 116, 091801 (2016).
- [37] A. Greljo, G. Isidori, J. M. Lindert, and D. Marzocca, Pseudo-observables in electroweak Higgs production, Eur. Phys. J. C 76, 158 (2016).
- [38] A. V. Gritsan, R. Röntsch, M. Schulze, and M. Xiao, Constraining anomalous Higgs boson couplings to the heavy flavor fermions using matrix element techniques, Phys. Rev. D 94, 055023 (2016).
- [39] LHC Higgs Cross Section Working Group, Handbook of LHC Higgs Cross Sections: 4. Deciphering the Nature of the Higgs Sector, CERN Yellow Rep. Monogr. 2 (2017).
- [40] C. Hartmann and M. Trott, Higgs Decay to Two Photons at One Loop in the Standard Model Effective Field Theory, Phys. Rev. Lett. 115, 191801 (2015).
- [41] S. Dawson and P. P. Giardino, Higgs decays to ZZ and $Z\gamma$ in the standard model effective field theory: An NLO analysis, Phys. Rev. D **97**, 093003 (2018).
- [42] A. Dedes, M. Paraskevas, J. Rosiek, K. Suxho, and L. Trifyllis, The decay $h \rightarrow \gamma \gamma$ in the standard-model effective field theory, J. High Energy Phys. 08 (2018) 103.
- [43] S. Dawson and P. P. Giardino, Electroweak corrections to Higgs boson decays to $\gamma\gamma$ and W^+W^- in standard model EFT, Phys. Rev. D **98**, 095005 (2018).
- [44] I. Brivio, T. Corbett, and M. Trott, The Higgs width in the SMEFT, J. High Energy Phys. 10 (2019) 056.
- [45] A. V. Gritsan, J. Roskes, U. Sarica, M. Schulze, M. Xiao, and Y. Zhou, New features in the JHU generator framework: Constraining Higgs boson properties from on-shell and off-shell production, Phys. Rev. D 102, 056022 (2020).
- [46] ATLAS Collaboration, Evidence for the spin-0 nature of the Higgs boson using ATLAS data, Phys. Lett. B 726, 120 (2013).
- [47] CMS Collaboration, Measurement of the properties of a Higgs boson in the four-lepton final state, Phys. Rev. D 89, 092007 (2014).
- [48] CMS Collaboration, Constraints on the spin-parity and anomalous HVV couplings of the Higgs boson in proton collisions at 7 and 8 TeV, Phys. Rev. D **92**, 012004 (2015).

- [49] CMS Collaboration, Limits on the Higgs boson lifetime and width from its decay to four charged leptons, Phys. Rev. D **92**, 072010 (2015).
- [50] ATLAS Collaboration, Study of the spin and parity of the Higgs boson in diboson decays with the ATLAS detector, Eur. Phys. J. C **75**, 476 (2015).
- [51] ATLAS Collaboration, Test of *CP* invariance in vectorboson fusion production of the Higgs boson using the Optimal Observable method in the ditau decay channel with the ATLAS detector, Eur. Phys. J. C **76**, 658 (2016).
- [52] CMS Collaboration, Combined search for anomalous pseudoscalar HVV couplings in $VH(H \rightarrow b\bar{b})$ production and $H \rightarrow VV$ decay, Phys. Lett. B **759**, 672 (2016).
- [53] CMS Collaboration, Constraints on anomalous Higgs boson couplings using production and decay information in the four-lepton final state, Phys. Lett. B 775, 1 (2017).
- [54] ATLAS Collaboration, Measurement of inclusive and differential cross sections in the $H \to ZZ^* \to 4\ell$ decay channel in pp collisions at $\sqrt{s} = 13$ TeV with the ATLAS detector, J. High Energy Phys. 10 (2017) 132.
- [55] ATLAS Collaboration, Measurement of the Higgs boson coupling properties in the $H \to ZZ^* \to 4\ell$ decay channel at $\sqrt{s} = 13$ TeV with the ATLAS detector, J. High Energy Phys. 03 (2018) 095.
- [56] ATLAS Collaboration, Measurements of Higgs boson properties in the diphoton decay channel with 36 fb⁻¹ of pp collision data at $\sqrt{s} = 13$ TeV with the ATLAS detector, Phys. Rev. D **98**, 052005 (2018).
- [57] CMS Collaboration, Measurements of the Higgs boson width and anomalous HVV couplings from on-shell and off-shell production in the four-lepton final state, Phys. Rev. D **99**, 112003 (2019).
- [58] CMS Collaboration, Constraints on anomalous HVV couplings from the production of Higgs bosons decaying to τ lepton pairs, Phys. Rev. D 100, 112002 (2019).
- [59] ATLAS Collaboration, Test of CP invariance in vector-boson fusion production of the Higgs boson in the H $\rightarrow \tau\tau$ channel in proton–proton collisions at $\sqrt{s}=13$ TeV with the ATLAS detector, Phys. Lett. B **805**, 135426 (2020).
- [60] CMS Collaboration, Constraints on anomalous Higgs boson couplings to vector bosons and fermions in its production and decay using the four-lepton final state, Phys. Rev. D **104**, 052004 (2021).
- [61] T. Martini, R.-Q. Pan, M. Schulze, and M. Xiao, Probing the *CP* structure of the top quark Yukawa coupling: Loop sensitivity versus on-shell sensitivity, Phys. Rev. D **104**, 055045 (2021).
- [62] A. Denner, S. Dittmaier, M. Pellen, and C. Schwan, Low-virtuality photon transitions $\gamma^* \to f\bar{f}$ and the photon-to-jet conversion function, Phys. Lett. B **798**, 134951 (2019).
- [63] A. Falkowski, Higgs basis: Proposal for an EFT basis choice for LHC HXSWG, Technical Report No. LHCHXSWG-INT-2015-001, 2015, https://cds.cern.ch/record/2001958.
- [64] S. Weinberg, Baryon and Lepton Nonconserving Processes, Phys. Rev. Lett. 43, 1566 (1979).
- [65] W. Buchmuller and D. Wyler, Effective Lagrangian analysis of new interactions and flavor conservation, Nucl. Phys. B268, 621 (1986).

- [66] C. N. Leung, S. T. Love, and S. Rao, Low-energy manifestations of a new interaction scale: Operator analysis, Z. Phys. C 31, 433 (1986).
- [67] A. Dedes, W. Materkowska, M. Paraskevas, J. Rosiek, and K. Suxho, Feynman rules for the standard model effective field theory in R_{ξ} -gauges, J. High Energy Phys. 06 (2017) 143.
- [68] B. Grzadkowski, M. Iskrzynski, M. Misiak, and J. Rosiek, Dimension-six terms in the standard model Lagrangian, J. High Energy Phys. 10 (2010) 085.
- [69] J. M. Campbell and R. K. Ellis, MCFM for the Tevatron and the LHC, Nucl. Phys. B, Proc. Suppl. 205, 10 (2010).
- [70] J. M. Campbell, R. K. Ellis, and C. Williams, Vector boson pair production at the LHC, J. High Energy Phys. 07 (2011) 018.
- [71] J. M. Campbell, R. K. Ellis, and C. Williams, Bounding the Higgs width at the LHC using full analytic results for $gg \rightarrow e^-e^+\mu^-\mu^+$, J. High Energy Phys. 04 (2014) 060.
- [72] J. M. Campbell and R. K. Ellis, Higgs constraints from vector boson fusion and scattering, J. High Energy Phys. 04 (2015) 030.
- [73] J. M. Campbell, R. K. Ellis, and W. T. Giele, A Multi-Threaded Version of MCFM, Eur. Phys. J. C 75, 246 (2015).
- [74] CMS Collaboration, Measurement of Higgs boson production and properties in the WW decay channel with leptonic final states, J. High Energy Phys. 01 (2014) 096.
- [75] CMS Collaboration, Constraints on the Higgs boson width from off-shell production and decay to Z-boson pairs, Phys. Lett. B **736**, 64 (2014).
- [76] CMS Collaboration, Observation of the diphoton decay of the Higgs boson and measurement of its properties, Eur. Phys. J. C 74, 3076 (2014).
- [77] CMS Collaboration, Search for a Higgs boson in the mass range from 145 to 1000 GeV decaying to a pair of W or Z bosons, J. High Energy Phys. 10 (2015) 144.
- [78] CMS Collaboration, Measurements of $t\bar{t}H$ Production and the *CP* Structure of the Yukawa Interaction between the Higgs Boson and Top Quark in the Diphoton Decay Channel, Phys. Rev. Lett. **125**, 061801 (2020).
- [79] CMS Collaboration, Search for a new scalar resonance decaying to a pair of Z bosons in proton-proton collisions at $\sqrt{s} = 13$ TeV, J. High Energy Phys. 06 (2018) 127; 03 (2019) 128(E).
- [80] CMS Collaboration, Search for a heavy Higgs boson decaying to a pair of W bosons in proton-proton collisions at $\sqrt{s} = 13$ TeV, J. High Energy Phys. 03 (2020) 034.
- [81] A. Falkowski, B. Fuks, K. Mawatari, K. Mimasu, F. Riva, and V. Sanz, Rosetta: An operator basis translator for standard model effective field theory, Eur. Phys. J. C 75, 583 (2015).
- [82] L3 Collaboration, Search for anomalous couplings in the Higgs sector at LEP, Phys. Lett. B 589, 89 (2004).
- [83] H. Khanpour, S. Khatibi, and M. M. Najafabadi, Probing Higgs boson couplings in $H + \gamma$ production at the LHC, Phys. Lett. B **773**, 462 (2017).
- [84] L. Shi, Z. Liang, B. Liu, and Z. He, Constraining the anomalous Higgs boson coupling in $H + \gamma$ production, Chin. Phys. C **43**, 043001 (2019).

- [85] I. Brivio, Y. Jiang, and M. Trott, The SMEFTsim package, theory and tools, J. High Energy Phys. 12 (2017) 070.
- [86] J. Alwall, R. Frederix, S. Frixione, V. Hirschi, F. Maltoni, O. Mattelaer, H.-S. Shao, T. Stelzer, P. Torrielli, and M. Zaro, The automated computation of tree-level and next-to-leading order differential cross sections, and their matching to parton shower simulations, J. High Energy Phys. 07 (2014) 079.
- [87] A. Denner, S. Dittmaier, and A. Mück, PROPHECY4F 3.0: A Monte Carlo program for Higgs-boson decays into four-fermion final states in and beyond the standard model, Comput. Phys. Commun. 254, 107336 (2020).
- [88] A. Denner, S. Dittmaier, S. Kallweit, and A. Mück, HAWK 2.0: A Monte Carlo program for Higgs production in vector-boson fusion and Higgs strahlung at hadron colliders, Comput. Phys. Commun. 195, 161 (2015).
- [89] Particle Data Group Collaboration, Review of particle physics, Prog. Theor. Exp. Phys. 2020, 083C01 (2020).
- [90] NNPDF Collaboration, Parton distributions for the LHC Run II, J. High Energy Phys. 04 (2015) 040.
- [91] CMS Collaboration, Measurement of the weak mixing angle with the Drell-Yan process in proton-proton collisions at the LHC, Phys. Rev. D **84**, 112002 (2011).
- [92] A. Djouadi, J. Kalinowski, M. Mühlleitner, and M. Spira, HDECAY: Twenty + + years after, Comput. Phys. Commun. **238**, 214 (2019).
- [93] D. Fontes, M. Mühlleitner, J. C. Romão, R. Santos, J. P. Silva, and J. Wittbrodt, The C2HDM revisited, J. High Energy Phys. 02 (2018) 073.
- [94] I. Low, J. Lykken, and G. Shaughnessy, Have we observed the Higgs (Imposter)?, Phys. Rev. D 86, 093012 (2012).
- [95] R. Contino, M. Ghezzi, C. Grojean, M. Mühlleitner, and M. Spira, eHDECAY: An implementation of the Higgs effective Lagrangian into HDECAY, Comput. Phys. Commun. 185, 3412 (2014).
- [96] A. Bredenstein, A. Denner, S. Dittmaier, and M. M. Weber, Precise predictions for the Higgs-boson decay $H \rightarrow WW/ZZ \rightarrow 4$ leptons, Phys. Rev. D **74**, 013004 (2006).
- [97] A. Denner, S. Dittmaier, S. Kallweit, and A. Muck, Electroweak corrections to Higgs-strahlung off W/Z bosons at the Tevatron and the LHC with HAWK, J. High Energy Phys. 03 (2012) 075.
- [98] J. Alwall *et al.*, A standard format for Les Houches event files, Comput. Phys. Commun. **176**, 300 (2007).
- [99] F. Granata, J. M. Lindert, C. Oleari, and S. Pozzorini, NLO QCD + EW predictions for HV and HV +jet production including parton-shower effects, J. High Energy Phys. 09 (2017) 012.
- [100] S. Eidelman and F. Jegerlehner, Hadronic contributions to (g-2) of the leptons and to the effective fine structure constant $\alpha(M_z^2)$, Z. Phys. C **67**, 585 (1995).
- [101] A. Keshavarzi, D. Nomura, and T. Teubner, Muon g-2 and $\alpha(M_Z^2)$: A new data-based analysis, Phys. Rev. D **97**, 114025 (2018).
- [102] S. Frixione, P. Nason, and C. Oleari, Matching NLO QCD computations with parton shower simulations: The POW-HEG method, J. High Energy Phys. 11 (2007) 070.
- [103] CMS Collaboration, Measurements of production cross sections of the Higgs boson in the four-lepton final state in

- proton-proton collisions at $\sqrt{s} = 13$ TeV, Eur. Phys. J. C **81**, 488 (2021).
- [104] A. S. Nemirovsky and D. B. Yudin, Problem Complexity and Method Efficiency in Optimization (Wiley, New York, 1983).
- [105] T. Chen and T.-Y. Li, Homotopy continuation method for solving systems of nonlinear and polynomial equations, Commun. Inf. Syst. 15, 119 (2015).
- [106] T. Chen, T.-L. Lee, and T.-Y. Li, Hom4PS-3: A parallel numerical solver for systems of polynomial equations based on polyhedral homotopy continuation methods, in *Mathematical Software—ICMS 2014*, edited by H. Hong and C. Yap Lecture Notes in Computer Science Vol. 8592 (Springer, Berlin, Heidelberg, 2014), pp. 183–190, 10.1007/978-3-662-44199-2 30.
- [107] T. Chen, T.-L. Lee, and T.-Y. Li, Mixed cell computation in Hom4PS-3, J. Symb. Comput. 79, 516 (2017).

- [108] Gurobi Optimization, LLC, Gurobi Optimizer Reference Manual (2018), https://www.gurobi.com/products/ gurobioptimizer/.
- [109] A. Abbasabadi, D. Bowser-Chao, D. A. Dicus, and W. W. Repko, Higgs-photon associated production at hadron colliders, Phys. Rev. D 58, 057301 (1998).
- [110] ATLAS Collaboration, Search for heavy resonances decaying to a photon and a hadronically decaying Z/W/H boson in pp collisions at $\sqrt{s} = 13$ TeV with the ATLAS detector, Phys. Rev. D **98**, 032015 (2018).
- [111] ATLAS Collaboration, Search for Heavy Resonances Decaying into a Photon and a Hadronically Decaying Higgs Boson in pp Collisions at $\sqrt{s} = 13$ TeV with the ATLAS Detector, Phys. Rev. Lett. **125**, 251802 (2020).
- [112] M. Cepeda *et al.*, Higgs Physics at the HL-LHC and HE-LHC, CERN Yellow Rep. Monogr. **7**, 221 (2019).